Deuterium induces a distinctive *Escherichia coli* proteome that correlates with the reduction in growth rate

Received for publication, November 29, 2018, and in revised form, December 13, 2018 Published, Papers in Press, December 13, 2018, DOI 10.1074/jbc.RA118.006914

Christian Opitz[‡], **Erik Ahrné**[‡], **Kenneth N. Goldie**[§], **Alexander Schmidt**[‡], **and Stephan Grzesiek**[‡1]

From the [‡]*Biozentrum, University of Basel, CH-4056 Basel, Switzerland and* [§]*Center for Cellular Imaging and Nanoanalytics, Biozentrum, University of Basel, CH-4058 Basel, Switzerland*

Edited by Wolfgang Peti

Substitution of protium (H) for deuterium (D) strongly affects biological systems. Whereas higher eukaryotes such as plants and mammals hardly survive a deuterium content of >30%, many microorganisms can grow on fully deuterated media, albeit at reduced rates. Very little is known about how the H/D replacement influences life at the systems level. Here, we used MS-based analysis to follow the adaptation of a large part of the *Escherichia coli* proteome from growth on a protonated full medium, over a protonated minimal medium, to a completely deuterated minimal medium. We could quantify >1800 proteins under all conditions, several 100 of which exhibited strong regulation during both adaptation processes. The adaptation to minimal medium strongly up-regulated amino acid synthesis and sugar metabolism and down-regulated translational proteins on average by 9%, concomitant with a reduction in growth rate from 1.8 to 0.67 h^{-1}. In contrast, deuteration caused a very wide proteomic response over many cell functional categories, together with an additional down-regulation of the translational proteins by 5%. The latter coincided with a further reduction in growth rate to 0.37 h^{-1}, revealing a clear linear correlation between growth rate and abundance of translational proteins. No significant morphological effects are observed under light and electron microscopies. Across all protein categories, about 80% of the proteins up-regulated under deuteration are enzymes with hydrogen transfer functions. Thus, the H/D kinetic isotope effect appears as the major limiting factor of cellular functions under deuteration.

Because of the large relative mass change, the isotopes of hydrogen differ more in chemical properties than the isotopes of any other element (1). Biological effects of the exchange of protium (H)[2] to deuterium (D) have been described since very early (1–5) after the discovery of deuterium in 1932 (6). It is well-known that higher plants and even the simplest animals are severely affected by growth on D_2O and do not survive concentrations higher than ~30–50% (1, 4). In contrast, lower organisms such as bacteria, algae, yeast, and molds and some other eukaryotic unicellular organisms can be adapted, albeit at reduced growth rates, to life on 100% D_2O resulting in the stable deuteration of their cellular components (1, 4, 7). Important applications of deuteration comprise labeling for NMR, neutron scattering, and MS, increasing the stability of pharmacological compounds as well as the study of fundamental determinants of kinetics and stability in biomolecular systems. Although it is obvious that the detrimental biological effects of deuteration are based on the altered physicochemical properties of deuterated compounds, no particular biomolecular function has been identified that would preclude life under deuteration.

The higher deuteron mass affects physicochemical behavior by two prominent effects: (i) it reduces the length of single bonds to heavy atoms and (ii) it slows the rates of hydrogen transfer reactions. The shortening of heavy atom to deuteron single bonds on the order of 0.005 Å (8–10) relative to protium bonds is the result of the anharmonicity of single-bond vibrations. In turn, the shorter bonds exhibit lower bond polarization and reduced acidity. Thus the p*K* of water increases from 13.995 in H_2O to 14.951 in D_2O (11), whereas the p*K* values of single deprotonation reactions for common acids increase typically by about 0.4 (12). The shortening of the covalent bond length of hydrogen bond (H-bond) donors also leads to an increase of the donor to acceptor distance in H-bonds on the order of 0.01–0.04 Å, commonly known as the classical Ubbelohde effect (13), and a slight weakening of H-bond orbital overlap (14). In contrast to these relatively small equilibrium effects, kinetic isotope effects (KIEs) in hydrogen transfer reactions can be considerably larger. The primary KIEs defined by the ratio k_H/k_D of the hydron transfer rates are typically in the range of 1–10, which can be explained by semiclassical theories via the differences in zero point vibrations (15). However, KIEs may also reach values of up to ~80 because of quantum mechanical tunneling (16, 17).

The consequences of these physicochemical effects on the cellular function of biomolecules are not well-understood. D_2O and deuteration certainly affect the stability of biomolecules, but the size of the effects is relatively small. Thus D_2O solvent marginally increases the melting temperature of dsDNA by about 2 K (18, 19) and the phase transition temperatures in

This work was supported by Swiss National Science Foundation Grants 31-149927 and 31-173089 (to S. G.). The authors declare that they have no conflicts of interest with the contents of this article.
This article contains Figs. S1–S4 and Tables S1–S4.
The MS proteomics data have been deposited to the ProteomeXchange Consortium via the PRIDE partner repository with the data set identifier PXD009736.
[1] To whom correspondence should be addressed. Tel.: 41 61 267 2100; Fax: 41 61 267 2109; E-mail: Stephan.Grzesiek@unibas.ch.
[2] The abbreviations used are: H, protium; D, deuterium; KIE, kinetic isotope effect; H-bond, hydrogen bond; TCA, tricarboxylic acid; COG, Clusters of Orthologous Groups (database); GO, Gene Ontology (database); SDC, sodium deoxycholate.

lipids by about 1 K (20) and usually, but not always, increases the thermal stability of proteins (21–28). In contrast, covalent deuteration reduces the thermal stability of proteins (21, 29). Interestingly, deuteration of phospholipids also decreases the temperature of the gel to liquid crystalline phase transition by 4–5 K and lipid structural order (30, 31). These observations for both proteins and lipids hint at a reduction of attractive van der Waals interactions under deuteration. Compared with these moderate changes in stability, the stronger kinetic isotope effects, *i.e.* the reduction of hydrogen transfer rates (15, 17), are likely to be more critical for cellular function, but comprehensive studies are lacking and descriptions have remained largely phenomenological.

Early microscopic observations suggested that D_2O affects the size and morphology of cells and microorganisms (1, 2, 4) and chloroplast ordering in algae (1) and causes mitotic arrest (4, 32), which in microorganisms may be overcome by adaptation (4). Most of these observations have not been analyzed further by modern high-resolution techniques. Of note, the inhibition of mitosis has been investigated by immunofluorescence microscopy (33) and *in vitro* assays of isolated microtubules (34). The latter show increased microtubule polymerization and decreased rates of microtubule growth and GTP hydrolysis in D_2O (34). On the level of general cellular functions, a reduction of protein translation and an accumulation of mRNA induced by D_2O have been observed in cell-free protein expression assays (35). Besides one report indicating effects of D_2O on the tricarboxylic acid (TCA) cycle and the C_1 metabolic pathways in *Escherichia coli* (36), no systematic metabolomics studies have been undertaken.

With the advent of modern omics techniques and the increase in resolution of structural techniques, a much more comprehensive description of the deuteration effect on life becomes feasible. As a first step toward such a description at the system level, we have followed the morphology and the response of the *E. coli* proteome during adaptation to a highly deuterated (≥99% atom-D) minimal growth medium. As a byproduct, we have also characterized the proteome response from a protonated full medium to a protonated minimal medium. These responses occur within several hours and are faster than a possible modification of the genome by genetic selection. Very strong and distinct proteome changes accompanied by reductions in growth rates are observed for both processes, whereas cell size and subcellular organization remain largely unaffected. The transition from full to minimal medium predominantly up-regulates proteins involved in amino acid synthesis and glucose utilization, but down-regulates translational proteins. The change to the deuterated medium further reduces translational proteins in agreement with the further reduced growth rate. In contrast to the adaptation to minimal medium, the changes under deuteration are much more widespread and occur across almost all protein functional categories. Very often these changes affect enzymes involved in hydrogen transfer reactions. Thus the KIE appears as the major mechanism to influence and limit cellular function under deuteration.

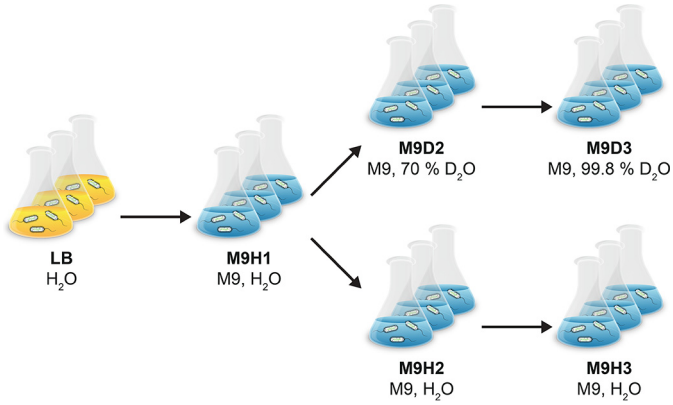

Figure 1. Adaptation of *E. coli* to growth in minimal and deuterated medium. Cells initially grown in protonated LB medium were transferred to protonated M9 minimal medium (M9H1). Subsequently, cells were either transferred to 70% D_2O (M9D2) and finally to perdeuterated M9 medium (M9D3) or retained in protonated M9 medium for two consecutive cultures (M9H2, M9H3). Each adaptation was performed for typically five generations in exponentially growing cultures.

Results

Adaptation of E. coli to growth in a deuterated medium

To study the effect of a deuterated environment on *E. coli* under well-controlled conditions, we compared growth on protonated and deuterated minimal media, which can be easily generated from D_2O and deuterated glucose as the sole hydrogen sources (besides trace amounts of vitamins and EDTA). Very reproducible adaptation of *E. coli* to such a highly deuterated (≥99%) environment was achieved in a stepwise manner (Fig. 1). Cells were initially seeded in protonated full (LB) medium and then transferred sequentially to protonated M9 minimal medium (M9H1), 70% D_2O M9 medium (M9D2), and finally perdeuterated M9 medium (99.8% D_2O, 97% deuterated glucose-d_7, M9D3). At each step, cells were grown within the exponential phase to an A_{600} of about 0.3–0.6 for typically five generations. For a stringent comparison, protonated M9H3 cultures were also generated as two consecutive cultures in protonated M9 medium from the M9H1 cells to match the total number of generations to the M9D3 cultures. To study the influence of the growth phase, samples for analysis were taken both from the exponential phase as well as from an extended cultivation of the cells to the early stationary phase ($A_{600} \geq 1.2$, Table S1). The transfer to the minimal and deuterated medium increased the growth rate (= ln(2)/generation time) from 1.8 ± 0.2 h^{-1} (LB), over 0.67 ± 0.02 h^{-1} (M9H1 and M9H3) to 0.37 ± 0.01 h^{-1} (M9D3). The nearly 2-fold decrease in growth rate in the deuterated medium provides manifest evidence of the severe deuterium isotope effects on *E. coli* cellular functions.

Cell shape analysis by light microscopy and cryo-EM

As early reports indicated strong changes in morphology and cell size of microorganisms induced by D_2O (1, 4), we sought to investigate this phenomenon by modern microscopic techniques. Cells from exponentially grown M9H3 and M9D3 cultures were indistinguishable with respect to their general appearance by phase-contrast light microscopy (Fig. 2*A*). A quantitative analysis (Fig. 2*B*) revealed a slight decrease in mean length (2.60 ± 0.02 μm → 2.41 ± 0.02 μm) and a slight increase

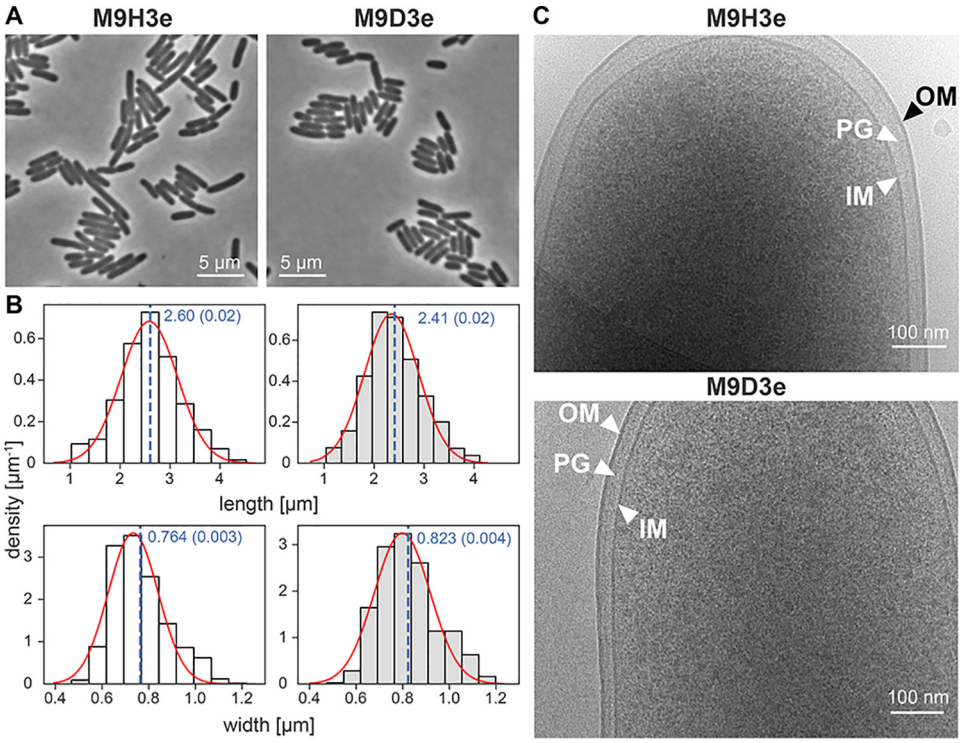

Figure 2. Microscopic analysis of *E. coli* cells and their cell size parameters obtained from exponentially grown protonated (M9H3) and deuterated (M9D3) minimal medium cultures. *A,* phase-contrast light micrographs of *E. coli* attached to agar slides. *B*, distributions of mean cell length (*upper panel*) and cell width (*lower panel*) for cultures shown in *A*. Mean values with their corresponding standard errors (in parentheses) are indicated by *dashed blue lines*. Fits of the binned cell size parameters to a Gaussian distribution are displayed as *solid red lines*. *C,* cryo-EMs of plunge-frozen samples obtained from cultures shown in *A*. Clearly observable cell organelles include the cell inner membrane (*IM*), the peptidoglycan layer (*PG*), as well as the outer membrane (*OM*).

in mean width (0.764 ± 0.003 μm → 0.823 ± 0.004 μm) because of the change from protonated to deuterated medium. These changes are minor relative to the observed variations of length and width within the cell populations (0.4 μm, 0.1 μm). To detect changes at higher resolution, we also analyzed plunge-frozen samples by cryo-EM. For both cultures, inner membrane, peptidoglycan layer, as well as the outer membrane were distinctly observable in the micrographs (Fig. 2*C*), but again indicated a very similar overall organization and size of the cell envelope in M9D3e compared with M9H3e cultures. Also, no particular differences are observable in the cellular interior and its visible ribosomal particles. Thus our results, in contrast to the early literature reports, indicate that growth on the deuterated medium does not induce strong effects on shape and cellular organization of *E. coli*.

Proteomics data quality and biological variability

To follow the adaptation to D_2O at a detailed molecular level, we have analyzed the proteome of *E. coli* grown on protonated full (LB), protonated minimal (M9H3), and deuterated minimal (M9D3) media using shotgun LC-MS/MS of proteolyzed samples. A high accuracy of the relative protonated and deuterated protein abundances was obtained by combining protonated and deuterated proteolyzed samples as 1:1 mixtures into single samples for combined LC-MS/MS. The acquired LC-MS/MS data were subjected to a combined search and quantification of protonated and deuterated peptides taking into account the reduced retention times of deuterated peptides yielding a high correlation between the detected protonated and deuterated proteins ($r^2 = 0.859$, see "Materials and methods" for details). To verify the accuracy of the detected mass intensity changes, we analyzed different ratios of protonated and deuterated peptide mixtures in the range of 0.1 to 10 (Fig. 3*A*). The ratios of detected deuterated *versus* protonated mass intensities showed an excellent linear correlation ($r^2 = 0.9999$) with the relative input concentrations of deuterated and protonated peptides. Thus our detection procedure accurately determines relative abundances of deuterated and protonated proteins over at least two orders of magnitude.

In total 1849 proteins were detected in common among all media conditions for samples obtained from the exponential- and also stationary-phase cultures (denoted by the appendices "e" and "s", respectively). Triplicate, independent cell cultures yielded very good reproducibility of the protein abundances with very similar distributions of their coefficients of variation (CV, relative standard deviations) for all conditions and median CV values in the 10% range (Fig. 3*B*).

A comparison between the different conditions showed highly significant effects. Thus 496 proteins exhibited at least 2-fold abundance changes with a q-value ≤ 0.01 when moving from the LB medium (LBe) to the protonated minimal medium (M9H3e) (Fig. 3*C*, *left panel*). The subsequent adaptation to the deuterated (M9D3e) minimal medium caused similarly strong changes for 384 proteins (Fig. 3*C*, *right panel*). Within these sets of regulated proteins, 143 are common between the adaptations from LBe to M9H3e and from M9H3e to M9D3e. Very similar abundance changes were observed between stationary-phase

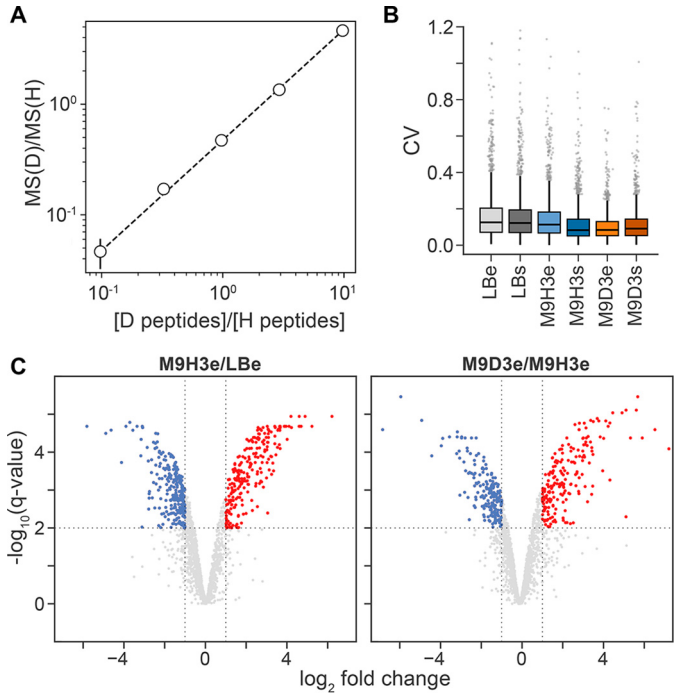

Figure 3. Linearity test and statistical quality of proteomics data on the *E. coli* adaptation to minimal and deuterated media. *A,* linearity test of detected deuterated MS intensities in mixed samples of protonated and deuterated *E. coli* peptide solutions. Ratios of summed deuterated and protonated detected intensities MS(D)/MS(H) are plotted against the ratio [D]/[H] of protonated and deuterated input peptide concentrations. The *dashed line* corresponds to a linear fit of all points with MS(D)/MS(H) = 0.475 [D]/[H] (r^2 = 0.9999). *B,* coefficients of variation (relative standard deviations, CVs) of the protein abundance data. *C,* $\log_2$ fold changes in protein abundance and their statistical significance (*q*-value) in the proteomes of *E. coli* cells grown in protonated M9 minimal *versus* protonated LB medium (M9H3e/LBe, *left panel*) and deuterated *versus* protonated minimal medium (M9D3e/M9H3e, *right panel*), respectively.

LBs and M9H3s as well as M9H3s and M9D3s cultures. The intensities and statistics of all detected proteins are listed in Table S2.

Principal component analysis reveals unique proteomes in full, minimal, and deuterated media

A principal component analysis of the total variations of protein abundances reveals that all three conditions of full (LB), protonated minimal (M9H3), and deuterated minimal (M9D3) media are separated into distinct clusters within the first and second principal components (Fig. 4). The high reproducibility within the triplicate cell cultures indicates a uniform and robust adaptation to the different conditions. Variations between exponential- and stationary-phase cultures are also small within both minimal media conditions (M9H3e/s, M9D3e/s), but are larger for the protonated full medium (LBe/s). Interestingly the position of LBs within the first two principal components is located on a line from LBe toward M9H3e/s at about one fifth of their distance. This points at a nutrient limitation under the stationary LB conditions, which is similar to, but not yet as severe as in, M9 medium. In strong contrast, the positions of M9D3e/s are clearly not collinear with the line connecting LBe and M9H3e/s. Thus the proteome changes because of deuteration are highly distinct from those caused by the nutrient limitations of the minimal medium.

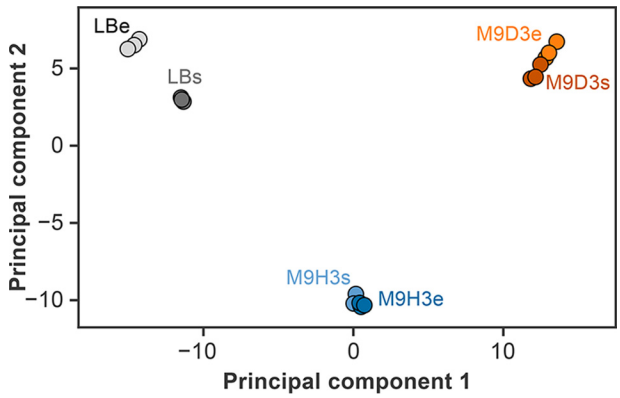

Figure 4. Principal component analysis of normalized protein abundances for different growth media. The proteome abundance vectors of *E. coli* grown in protonated full LBe/s, protonated (M9H3e/s), and deuterated M9 minimal (M9D3e/s) media strongly differ in their first two principal components, but are similar between respective exponential (e) and stationary phase (s) cultures.

Overall proteome resource allocation

Because the total of proteins detected by the present mass spectrometric analysis covers almost the entire cellular expressed protein content (37), the protein MS signal/total MS signal is a very good estimate of the cellular protein mass/total cellular protein mass (38). To obtain an overview of the proteome allocation to different functional categories, we summed the protein signals detected within the 22 categories of the Clusters of Orthologous Groups (COG) database (39) and normalized these values by the total detected MS signal. Across each condition, the largest fraction of the detected proteome belongs to the COG translation category J, which comprises the ribosomal proteins and amounts to 36% of the total protein mass for LBe (30% for LBs) (Fig. 5*A*). Upon change to protonated minimal medium (M9H3e/s), this fraction is reduced to 27%, and the second largest category E associated to amino acid metabolism is up-regulated to 13% from the 7% in LB. This is consistent with the absence of amino acids in the minimal medium, which need to be synthesized by *E. coli*. However, the reduced supply of amino acids apparently still limits translation and in consequence reduces the amount of proteins in category J. Similar-sized variations of this category in response to nutrient supply have been observed previously (37, 40). For instance, as compared with a glucose minimal medium, 9% of protein mass in *E. coli* was saved on amino acid synthesis in an LB medium and allocated to translation, which made the growth rate jump from 0.65 to 1.6 h^{-1}. In fact, a very good linear relation exists between the protein amount in category J and the growth rate where a 5% increase in J approximately increases the growth rate by 0.5 h^{-1} (37).

Compared with the protonated minimal medium (M9H3), the deuterated minimal medium (M9D3e/s) causes a further reduction of proteome allocation to the translation category J from 27 to 22%, which is again consistent with the observed further decrease in the cellular growth rate. Indeed a comparison of the proteome allocation to category J to observed growth rates in LBe, M9H3, and M9D3 (Fig. 5*B*) exactly reproduces the previously obtained linear relation (37). Only very minor variations occur in the other COG categories upon change to the

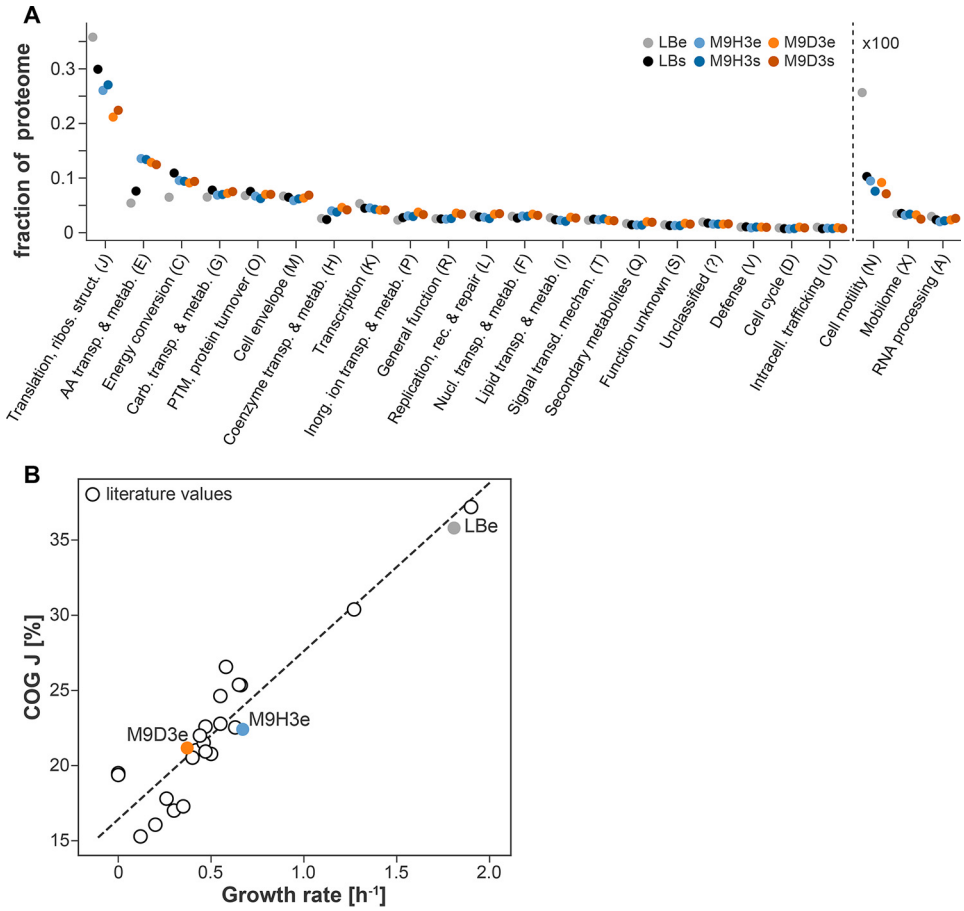

Figure 5. Protein resource allocation and growth rates for the different medium conditions. *A,* overall allocation of the detected proteins of *E. coli* cultures in the various growth media according to the 22 categories of the COG database. The detected protein abundances are normalized by the total abundance of all detected proteins for each condition. *B,* observed growth rates (Table S1) *versus* protein allocation to the translational class J for LBe, M9H3e, and M9D3e (*filled circles*). Additionally shown are values (*open circles*) for many further media conditions obtained previously by Schmidt *et al.* (37) using an identical analysis. The *dashed line* corresponds to a linear fit of all points with COG J [%] = 11.2 growth rate [h^{-1}] + 16.4 ($n = 25$, $r^2 = 0.922$).

deuterated medium. In particular, no significant change is observed for the amino acid metabolism (category E) proteins. Thus translation and growth under deuteration are apparently not limited by amino acid synthesis, otherwise one would expect an up-regulation of category E. Rather, translation and growth must be limited by other pathways.

Changes of the proteome specific to minimal medium

To identify specific cellular responses to the growth media, we have selected significantly regulated proteins from the total observed proteome changes in two different ways: (i) we selected the set of 30 most strongly regulated, individual proteins (set S1) and (ii) we clustered all detected proteins into functionally related classes according to the Gene Ontology (GO) database and identified the most strongly regulated classes. For a robust identification of the latter, only GO classes were considered, for which at least 75% of their contained proteins were detected with such low variation that they could be classified as either strongly regulated (at least 2-fold up or down) or as not strongly regulated (less than 2-fold). The entire GO class was then considered as strongly up- or down-regulated when at least 50% of its significantly detected proteins were at least 2-fold up- or down-regulated, respectively. A superset of significantly regulated proteins (set S2) was then created by merging set S1 with the more than 2-fold regulated proteins in the strongly regulated GO classes. Fig. 6 shows the set S1 of the 30 most strongly regulated proteins for the change from the LBe to the M9H3e minimal medium (Fig. 6*A*), a selection of the significantly regulated GO classes (Fig. 6*B*), and a histogram of set S2 according to the COG categories (Fig. 6*C*). All identified significant GO classes and the superset S2 of 154 significantly regulated proteins are given in Fig. S1 and Table S3, respectively. Note that here and in the following, only data from the exponential growth cultures were considered to exclude effects of nutrient and oxygen limitation in the stationary phase.

Consistent with the lack of amino acids, many of the most strongly up-regulated proteins in the minimal medium M9H3e (Fig. 6, *A* and *C*) are part of the COG amino acid metabolism category E and comprise proteins involved in biosynthesis of branched amino acids (*livJ, livK, ilvN, leuA,* gene names are used for clarity), lysine (*lysC*), methionine (*metE, metF*), tryptophan (*trpD*), binding of glutamate/aspartate (*gltI*), as well as peptide chemotaxis (*dppA*) (41). Conversely, proteins associated with amino acid degradation and import (*sdaB, sdaC, tdcG*) as well as peptide transmembrane (*dtpA*) and amine betaine (*proV*) transport are strongly (>10-fold) down-regulated.

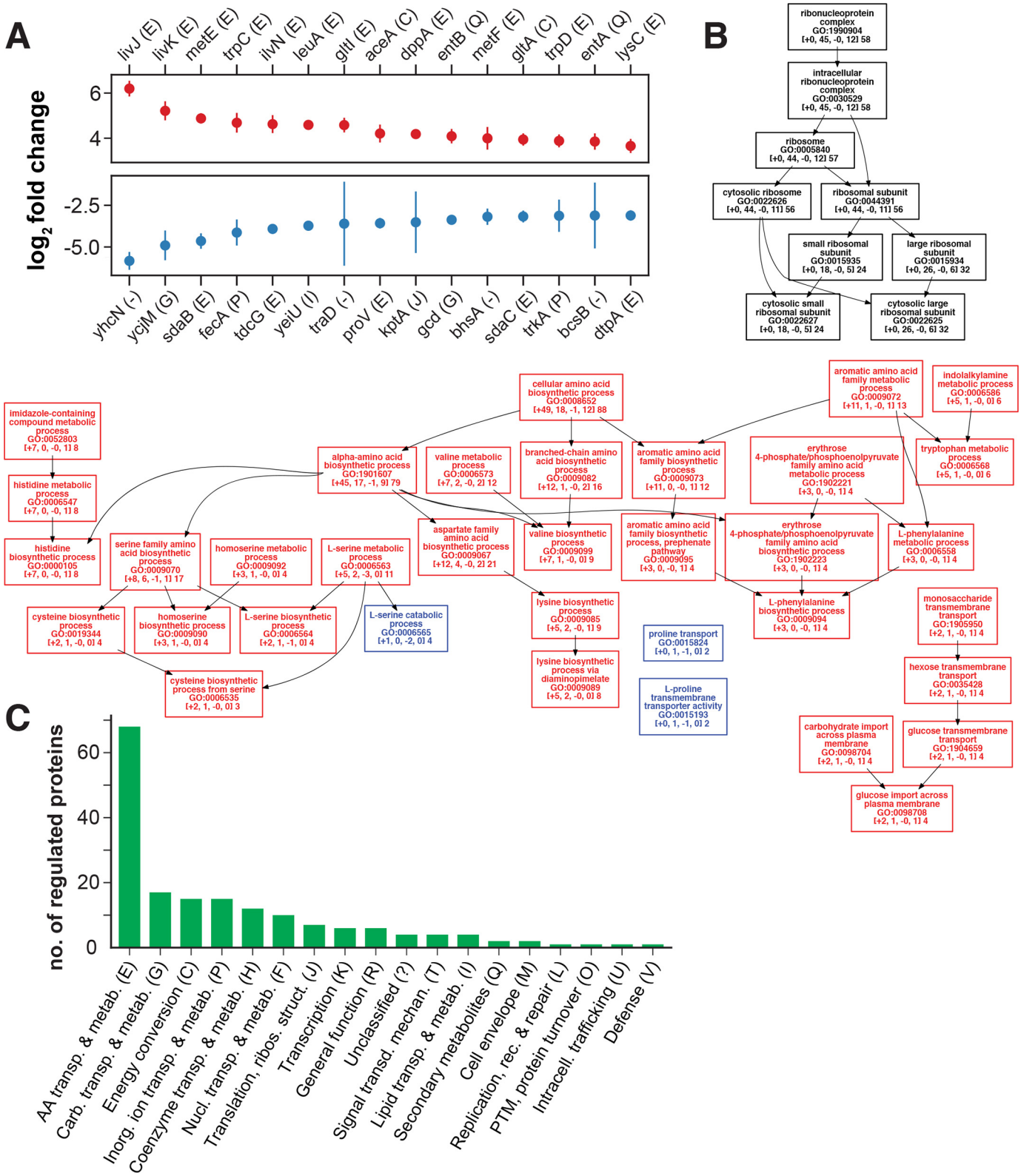

Figure 6. Functional analysis of proteome changes between *E. coli* cells grown in protonated M9 minimal (M9H3e) and protonated full (LBe) medium. *A*, $\log_2$ fold changes of the 30 most strongly regulated proteins and their assigned COG classes (in parentheses). *B*, selection of significantly regulated (*red*: up; *blue*: down) or significantly not-regulated (*black*) protein clusters identified by the GO classification (see text). The values in the last line of each GO class indicate from left to right: the number of significantly up-regulated (N_{up}), significantly not regulated ($N_{not\ regulated}$), significantly down-regulated (N_{down}), not significantly detected ($N_{not\ significant}$), as well as the total number of proteins in the class (N_{tot}). The complete set of identified significant GO classes is shown in Fig. S1. *C*, functional distribution of the superset S2 of strongly regulated proteins (see text) according to their COG classification.

The increase in amino acid synthesis is also very clearly visible in the very strong up-regulation of many GO classes (Fig. 6*B*) associated with *de novo* amino acid biosynthesis (*cellular amino acid biosynthetic process*, GO:0008652; *aromatic amino acid family process*, GO:0009072; and their subclasses). Conversely, proline transport (GO:0015193 and GO:0015824) is strongly down-regulated. Interestingly, 45 of the 58 proteins of the GO class assigned to the ribonucleoprotein complex (GO: 1990904) could be quantified reliably. All of them are less than 2-fold regulated, which is consistent with the moderate down-regulation of the total COG translation category J by about 25% (Fig. 5*A*).

Also consistent with the fact that glucose is the sole carbon source of the minimal medium, very strong up-regulation is observed for two proteins central to the citric acid cycle (*gltA*) and its glyoxylate shunt (*aceA*) (42, 43) (Fig. 6*A*). Conversely, the strong down-regulation of the membranous glucose dehydrogenase (*gcd*) is expected to increase the availability of glucose by the repression of its direct oxidation. Corresponding to this importance of glucose and its import from the medium, multiple GO classes assigned to active glucose import are strongly up-regulated (Fig. 6*B*). Further, notably regulated proteins comprise two strongly up-regulated proteins of the enterobactin biosynthesis pathway (*entA*, *entB*), which suggests an increase of siderophore-based iron uptake, as well as strongly down-regulated proteins associated with biofilm formation (*yhcN*, *bhsA*) and the associated biosynthesis of cellulose (*bcsB*) (44, 45). The reported repression of biofilm formation by glucose (46) corroborates this observation.

The discussed proteins are only a small fraction of all proteins regulated upon change to minimal medium. A comprehensive understanding will require detailed follow-up studies. However, the largest changes of the proteome are clearly directed to utilize glucose as an energy source and synthesize amino acids (Fig. 6*C*). The shortage of the latter apparently limits translation.

Changes of the proteome specific to deuterated minimal medium

The response to the change from protonated (M9H3e) to deuterated (M9D3e) minimal medium markedly differs from the change from full to minimal medium. The respective set S1 of the 30 most strongly regulated proteins (Fig. 7*A*) and superset S2 of 120 significantly regulated proteins (Fig. 7*C* and Table S4) span a much larger variety of functional COG categories than found for the latter. Correspondingly, the identified strongly regulated GO classes (shown as selection in Fig. 7*B* and in full in Fig. S2) also are highly diverse, albeit the individual classes are rather small and often only very few proteins are affected. Consistent with the moderate overall down-regulation (<20%) of the COG translation category J in the deuterated medium and similar to the findings for the minimal medium, also the well-detected ribonucleoprotein complex GO class is not strongly regulated (Fig. 7*B*). Thus neither the COG nor the GO classification reveals any single biological mechanism, which is dominantly affected by the deuterated medium.

The change to D_2O and deuteration of cellular compounds is expected to slow hydrogen transfer and to affect chemical equilibria as well as the stability of biomolecules and their assemblies. In search for such a connection, we analyzed the superset S2 of significantly regulated proteins (Table S4) according to their specific function described in the UniProt database. This analysis reveals that indeed most of the regulated proteins can be linked to these expected physicochemical effects. Many of them are associated with (i) hydrogen transfer reactions, (ii) redox reactions, or (iii) membrane transport. A further significant number of regulated proteins are involved in (iv) nucleic acid metabolism and (v) homeostasis, which is not immediately apparent from the COG and GO classifications. Histograms of the number of up- and down-regulated proteins associated with groups (i–v) are shown in Fig. 7*D*. The following paragraphs discuss specific findings.

Hydrogen transfer reactions

Hydrogen transfer occurs in all reactions involved in the synthesis or cleavage of polycarbon chains as well as phosphorylation and dephosphorylation. Important examples comprise glycolysis and glycogenesis in the carbohydrate metabolism, most intermediate steps of the TCA cycle, amino acid metabolism, nucleic acid metabolism, ATP-driven energy transfer, as well as phosphosignaling. These reactions are expected to be significantly slowed upon change to a deuterated medium. An increase in the respective enzyme concentrations will counteract this slowing of the reaction rates and may lead to a net compensation of effects.

Of the 120 significantly regulated proteins in set S2, 73 are more than 2-fold up-regulated (Table S4), 57 of which can be clearly associated with hydrogen transfer. Hence 78% of the up-regulated proteins are hydrogen transfer enzymes (Fig. 7*D*). This is significantly higher than their average of 55% (673 proteins) within the total of 1228 significantly regulated or significantly nonregulated proteins (Table S2). In contrast, the 26 down-regulated hydrogen transfer enzymes constitute only 55% of all 47 down-regulated proteins in set S2, agreeing with their average in the total set of significantly detected proteins. Thus the hydrogen transfer enzymes are significantly up-regulated under deuterated conditions in agreement with the hypothesis of a compensation for their reduced reaction rates.

Examples of the most strongly up-regulated proteins (Fig. 7*A*) are the sulfur transferase *tusB* (gene name used for clarity), the sucrose phosphorylase *ycjM*, the guanosine methylase *rlmA*, the ATPase and GSH importer *gsiA*, the phosphotransferase *chbB*, the phosphodiesterase *glpQ*, and the transaminase *gabT*. The inspection of most significantly up-regulated GO classes also reveals hydrogen transfer as the basic reaction of their up-regulated enzymes (Fig. S2 and Table S4). In particular, strong up-regulation occurs for *glgA*, *glgB*, *glgC*, *glgP* of the GO class *glycogen metabolic process* (GO:0005977, Fig. 7*B*), which synthesize glucan chains using ADP-glucose, catalyze the formation of glycosidic linkages, synthesize ADP-glucose, or have glycogen phosphorylase activity, respectively. Furthermore, the up-regulated *gldA* (*glycerol metabolic process*, GO:0006071) catalyzes the NAD-dependent oxidation of glycerol to dihydroxyacetone, *maeA* (*malic enzyme activity*, GO:0004470) is a malate dehydrogenase, *ddlA* (*D-alanine-D-alanine ligase activity*, GO:0008716) ligates D-alanine under ATP hydrolysis, and *fabB*

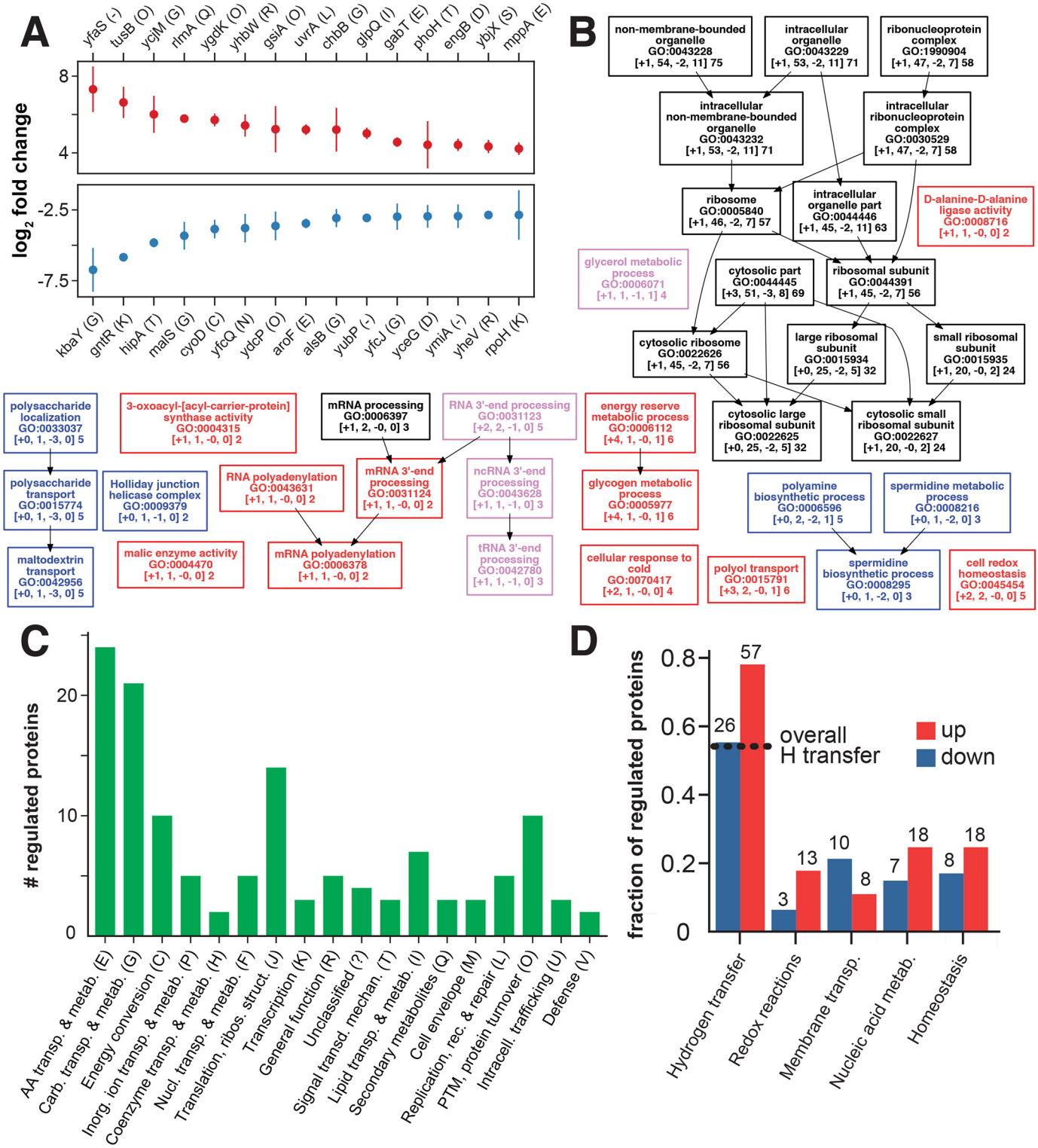

Figure 7. Functional analysis of proteome changes between *E. coli* cells grown in deuterated M9 minimal (M9D3e) and protonated M9 minimal (M9H3e) medium. *A*, $\log_2$ fold changes of the 30 most strongly regulated proteins and their assigned COG classes (in parentheses). *B*, selection of significantly regulated (*red*: up; *blue*: down) or significantly not regulated (*black*) protein clusters identified by the GO classification (see text). Several clusters (*magenta*) also showed significant combined up- and down-regulation ($(N_{up} + N_{down})/(N_{up} + N_{not\ regulated} + N_{down}) > 50\%$) of their detected proteins, albeit they were not significantly regulated in one direction (up or down). The complete set of identified significant GO classes is shown in Fig. S2. *C*, functional distribution of the superset S2 of strongly regulated proteins (see text) according to their COG classification. *D*, relative fractions of up- and down-regulated proteins in the set S2 according to their classification for (i) hydrogen transfer reactions, (ii) redox reactions, (iii) membrane transport, (iv) nucleic acid metabolism and (v) homeostasis (Table S4). The total number of proteins is indicated at the top. The *dashed line* indicates the fraction of hydrogen transfer enzymes identified in the total set of significantly regulated or significantly nonregulated proteins (Table S2).

(*3-oxoacyl-[acyl-carrier-protein] synthase activity*, GO:0004315) elongates fatty acids involving hydrogen transfer of histidine and cysteine residues in its active sites.

Redox reactions

Deuteration affects enzyme-catalyzed redox reactions by the KIE of proton-coupled electron transfer as well as by a change of redox equilibria (17, 47, 48). Electron transfer rates in D_2O are often slower (48), but can also be faster (47). Changes in the concentrations of the involved enzymes may counteract these variations. Indeed 16 of the 120 significantly regulated proteins in set S2 are involved in redox reactions, 13 of which are up-regulated (Fig. 7*D*). We observed *e.g.* strong up-regulation for the oxidoreductase *nrdH* and the transporter *cydD* essential for cytochrome biogenesis (*cell redox homeostasis*, GO:0045454), the sulfurtransferase subunit *tusB*, the oxidoreductase *yhbW*, and the poorly characterized sulfur acceptor *ygdK*. Conversely, the terminal oxidase *cyoD* associated with the cytochrome bo_3 complex is strongly down-regulated in the deuterated medium.

Membrane transport

The lower phase transition temperature and order of deuterated lipids (31) is expected to increase the fluidity of the deuterated cell membrane, thereby affecting stability and function of integral and membrane-associated proteins. The deuteration of the membrane proteins themselves as well as KIEs of reactions may further influence their function. We find that 10 of the 18 membrane transporters in set S2 are strongly down-regulated under deuteration (Fig. 7*D*). This includes the down-regulated *malE*, *malF*, *malK* (*maltodextrin transport*, GO:0042956) and the periplasmic *malS* that are involved in maltooligosaccharide transport, whereas *alsB* is required for binding and import of D-allose. Strong down-regulation also occurs for the outer membrane-bound *yfcJ* with unknown biological function. Conversely, *e.g. glpF* and *glpT* (*polyol transport*, GO:0015791) and the peptide transporter *mppA* are strongly up-regulated.

Nucleic acid metabolism

A relatively large number of enzymes involved in nucleic acid metabolism (25 in set S2, Fig. 7*D*) are differentially regulated in the deuterated medium. Because D_2O solvent causes only a minor increase (~2 K) in the melting temperature of DNA double strands (18, 19), again the KIE of hydrogen transfer reactions is a more likely cause for this regulation. Indeed, with the exception of the poorly characterized *ybjX*, the activity of all these proteins clearly involves hydrogen transfer reactions. Strong up-regulation is observed for 18 proteins, *e.g.* for the poly(A) polymerase I *pcnB* (*mRNA polyadenylation*, GO:0006378), the exoribonuclease *rph* (*tRNA 3′-end processing*, GO:0042780), the RNA helicase *deaD* (*cellular response to cold*, GO:0070417), the excinuclease *uvrA*, and the conserved DNA damage response protein *ybjX*. Conversely, strong down-regulation was observed *e.g.* for the exonuclease *rnt* (*tRNA 3′-end processing*, GO:0042780) and the helicase *recG* (*Holliday junction helicase complex*, GO:0009379), the carboxylase *speD*, and the propylamine transferase *speE* (*spermidine biosynthetic process*, GO:0008295). These changes of nucleic acid processing enzymes are expected to have a significant impact on transcription and translation in deuterated medium, which may correlate to the decreased growth rates.

Homeostasis

Not surprisingly, a notable number of proteins (26 in set S2, Fig. 7*D*) regulated in response to the deuterated medium are associated with homeostasis. Examples comprise the up-regulated trehalose-phosphate synthase *otsA*, the RNA helicase *deaD* (*cellular response to cold*, GO:0070417), and the essential cell cycle regulator *engB* (49). In contrast, down-regulation is observed for *hipA* and *ycfQ*, associated with dormancy and biofilm formation, the heat shock response protein *rpoH,* and the repressor of gluconate utilization *gntR*.

Discussion

We have shown that adaptation of *E. coli* from a full medium to a minimal medium and subsequently to a perdeuterated minimal medium can be followed by proteomics on more than 1800 proteins, several hundred of which are significantly regulated in both cases. A consistent up-regulation of proteins associated with amino acid synthesis and glucose utilization occurs in response to the minimal medium concomitant with a 9% overall down-regulation of proteins allocated to the translation category J and a slowing of the growth rate. The response to deuteration is highly distinct from the latter: It affects a much larger variety of proteins and a conventional functional classification by COG and GO annotations fails to identify any dominantly affected cellular mechanism. The total protein abundances in individual COG categories show only minor changes, but the further reduction by 5% of proteins in translation category J coincides with a further reduction in growth rate. The correlation between protein abundance in category J and growth rate reveals a clear linear dependence, which is in excellent agreement with earlier results for various nondeuterated growth media (37). Thus the reduced growth rate in perdeuterated medium and the reduced abundance of translational proteins are obviously connected; however, the cause for the down-regulation of the translational machinery is unclear. Because deuteration does not induce significant changes in the amino acid metabolism category E, the latter is apparently not the limiting factor for growth in the deuterated environment.

An in-depth analysis of the individual, regulated proteins reveals that most up-regulated proteins can be associated with hydrogen transfer and redox reactions, which are expected to be considerably slowed in a deuterated medium by the KIE. The up-regulation will counteract this negative effect of deuteration. Albeit such a connection between the deuterium KIE and the cellular response may have been expected in retrospect, no experimental data at the system level had been presented before. Further, notably affected proteins comprise membrane transporters and proteins involved in nucleic acid processing and homeostasis, which may be related to variations of membrane mechanical properties and the overall stability of nucleic acids and proteins under deuterated conditions.

The observed changes of the proteome occur within several hours, which is faster than a possible evolution of the genome. Additional insights into this regulation of the proteome could be obtained by transcriptomics, whereas the affected enzymatic

functions may be further assessed by metabolomics. Conversely, selection of fast-growing *E. coli* clones over a very large number of generations in a deuterated medium should lead to persistent changes in the genome and epigenome. It will be interesting to compare such genetic changes induced by directed evolution to the observed short-term adaption of the proteome.

Because other prokaryotes, yeast, and algae can also be adapted to perdeuterated media, identical approaches can be used to reveal the most conserved features of the deuteration response. For higher eukaryotes, including the biotechnologically important insect and mammalian cells, analogous experiments may be carried out up to their tolerated deuteration maximum of ~30–50% (1, 4, 50, 51). This may in particular identify the crucial factors which lead to the described arrest of the cell cycle during mitosis (4, 32–34, 51).

In summary, we have shown that systems biology approaches as exemplified by proteomics reveal highly significant changes in *E. coli* under deuteration. This should provide a starting point for studying fundamental determinants of kinetics and stability in biomolecular systems via the deuterium isotope effect as well as for the development of improved biotechnological deuteration methods.

Materials and methods

Growth media

Lysogeny broth (LB) medium was prepared from 5 g of yeast extract (BD Biosciences), 10 g tryptone (BD Biosciences), and 10 g NaCl dissolved in 1 liter of deionized water and sterilized by autoclaving. For the preparation of LB agar plates, 20 g of agar (BD Biosciences) were added to 1 liter of LB medium before autoclaving. Protonated M9 minimal medium without a carbon source was prepared by mixing 700 ml of deionized H_2O with 100 ml M9 salt solution (10×: 67.8 g/liter Na_2HPO_4, 30 g/liter KH_2PO_4, 5 g/liter NaCl in deionized H_2O), 1 g NH_4Cl, 10 ml of trace elements solution (100×: 5 g/liter EDTA, 0.5 g/liter $FeCl_3$, 84 mg/liter $ZnCl_2$, 10.3 mg/liter $CuCl_2$, 0.86 mg/liter $MnCl_2$, 5.5 mg/liter $CoCl_2$ in deionized H_2O), 0.3 ml 0.1 M $CaCl_2$, 1 ml 1 M $MgSO_4$, and 10 ml minimum Eagle's medium vitamin solution (100×). Finally, 20 ml 20% (w/v) glucose solution were added and the resulting solution was filled up to 1 liter with deionized H_2O. To prepare fractionally deuterated (70% D) M9 medium, 700 ml of this added H_2O were replaced by D_2O (99.8 atom % D). Deuterated (~99.8% D) M9 medium was prepared accordingly in 99.8% D_2O using stock solutions prepared from anhydrous powders in D_2O (99.8 atom % D) and 4 g/liter of glucose-1,2,3,4,5,6,6′-d_7 (97 atom % D). All growth media were filter-sterilized before use. Unless indicated otherwise, all chemicals were obtained from Sigma-Aldrich.

Growth and adaptation of E. coli

Cultures of *E. coli* BL21 (DE3) cells (genotype: F^-, *ompT*, *gal*, *dcm*, *lon*, *hsdSB*(rB^- mB^-), λ(*lacI*, *lacUV5-T7 gene 1*, *ind1*, *sam7*, *nin5*)) (52) were grown on a rotary shaker (220 rpm, 50 mm throw) at 37 °C in batches of 15 ml in 100-ml Erlenmeyer flasks to provide sufficient aeration. First, cultures grown to stationary phase in LB medium were used to inoculate protonated M9 medium at an A_{600} of 0.01. Subsequently, cells in M9 medium were grown for five generations (~5.2 h total, M9H1). Adaptation to deuterated medium was achieved by repeated subculturing. For this, M9H1 cells were separated from the supernatant by centrifugation at 5000 × *g* for 5 min and resuspended in (70% D) M9 medium at A_{600} of 0.01 to grow for five generations (~7.3 h total, M9D2). Finally, the M9D2 cultures were again centrifuged and transferred to (~99.8% D) M9 medium at A_{600} of 0.01 to grow for five generations (~9.3 h total, M9D3). To ensure comparability of cells grown in protonated M9 medium to the M9D3 cells, M9H1 cultures were further subcultured twice in fresh M9 medium, yielding a total number of 15 generations (M9H3).

Light microscopy and image analysis

Samples were prepared for phase contrast imaging by adsorbing 3 μl of culture on a thin LB agar patch (5 × 5 mm) placed on a microscopic slide, briefly dried, and protected by a coverslip. Phase images were acquired on a DeltaVision imaging system (GE Healthcare) equipped with an Olympus IX71 microscope, a CoolSNAP HQ2 CCD camera (Photometrics), and a 100×/1.4 NA Ph3 Plan-Apochromat oil immersion objective (Olympus). Z stacks were collected 0.2 μm apart to cover the full volume of the bacteria. Image feature classification was performed using ilastik (53). Subsequently, cell size parameters were calculated from the ilastik output by the CellProfiler software package (54).

EM

Samples were prepared for cryo-TEM by adsorbing 4 μl of the undiluted culture suspension onto lacey carbon film mounted on 300 mesh copper grids (Ted Pella, Inc., Redding, CA). Prior to adsorption, the grid was rendered hydrophilic by glow discharge for 15 s. The specimen was applied to the grid surface and after 3-min incubation the grid was blotted en face and quick-frozen in liquid ethane using a Leica EM GP automated plunging device (Leica Microsystems, Vienna, Austria). The frozen grids were transferred under liquid nitrogen and loaded into a Gatan 626 cryo-holder (Gatan, Pleasanton, CA), which was then inserted into the stage of a FEI Talos transmission electron microscope (FEI Company, Hillsboro, OR) operated at 200 kV. Imaging was performed at cryogenic temperatures (approximately −170 °C) in low-dose, bright-field mode. Electron micrographs were recorded digitally on a CETA 16 M 4k × 4k CMOS Camera (FEI Company, Hillsboro, OR) at nominal defocus values of approximately −5 to −7 μm. The electron dose for low-dose image acquisition was maintained at ~30 e/Å^2 per second.

Whole-cell lysis and tryptic digestion of E. coli

Samples for proteome analyses were collected from the cultures grown for five generations in LB medium, protonated M9 medium (M9H1), and deuterated M9 medium (M9D3) as well as 15 generations in protonated M9 medium (M9H3) by centrifugation at 20,000 × *g* (4 °C) for 5 min. The obtained cell pellets were flash-frozen in liquid nitrogen and stored at −80 °C until further processing. Cells were resuspended in 100 mM ammonium carbonate containing 2% sodium deoxycholate (SDC) and 5 mM tris(2-carboxyethyl)phosphine (TCEP lysis

buffer). The cells were lysed by combined harsh vortexing (3 × 30 s) and sonication (3 × 10 s, 0.5 duty cycle, and 100% amplitude) using a VialTweeter (Hielscher). Obtained lysates were heated to 95 °C for 10 min while shaking at 500 rpm, followed by centrifugation at 10,000 × *g* for 10 s to remove cell debris. The protein concentration in the supernatant was determined using a BCA assay kit (Thermo Fisher Scientific). Subsequently, samples were diluted in lysis buffer to yield a protein concentration of 5 μg/μl and alkylation was performed on 100 μg of total protein in a volume of 20 μl using 10 mM of freshly prepared iodoacetamide for 30 min at 25 °C in the dark. The excess of iodoacetamide was quenched by addition of 12 mM *N*-acetylcysteine.

For digestion, samples were diluted to yield a final SDC concentration of 1% using 100 mM ammonium carbonate. Subsequently, trypsin (Sigma-Aldrich) was added in a 1:50 enzyme/protein ratio (w/w) and digestion was performed overnight at 37 °C. The reaction was terminated by addition of 1% TFA, followed by centrifugation to remove SDC precipitate at 15,000 × *g* for 10 min (4 °C). Centrifugation was repeated once more and the obtained supernatant was used for solid phase extraction.

Peptides were desalted on a C18 reversed-phase spin column according to the supplier's manual (Macrospin, Harvard Apparatus). All samples were prepared in biological triplicates.

LC-MS/MS analysis

To achieve reliable relative quantification of protonated and deuterated *E. coli* peptide mixtures, they were mixed 1:1, based on their total peptide content determined by a Bradford assay, into a single sample for LC-MS/MS analysis. In detail, exponential (e) and stationary (s) peptide mixtures of each protonated condition (LBe/s, M9H1e/s, and M9H3e/s) were combined with the corresponding deuterated M9D3(e/s) peptide mixtures generating a total of 18 (9 for each growth phase) mixed MS samples.

Each sample was then subjected to LC-MS analysis using a dual pressure LTQ-Orbitrap Elite mass spectrometer connected to an electrospray ion source (Thermo Fisher Scientific) as described (55) with a few modifications. In brief, peptide separation was carried out using an EASY nLC-1000 system (Thermo Fisher Scientific) equipped with a RP-HPLC column (75 μm × 45 cm) packed in-house with C18 resin (ReproSil-Pur C18-AQ, 1.9 μm resin; Dr. Maisch GmbH, Ammerbuch-Entringen, Germany) using a linear gradient from 95% solvent A (0.15% formic acid, 2% acetonitrile) and 5% solvent B (98% acetonitrile, 0.15% formic acid) to 28% solvent B over 120 min at a flow rate of 0.2 μl/min. The data acquisition mode was set to obtain one high-resolution MS scan in the FT part of the mass spectrometer at a resolution of 240,000 full width at half-maximum (at m/z 400) followed by MS/MS scans in the linear ion trap of the 20 most intense ions. The charged state screening modus was enabled to exclude unassigned and singly charged ions and the dynamic exclusion duration was set to 30 s. The ion accumulation time was set to 300 ms (MS) and 50 ms (MS/MS).

Identification and label-free quantification of protonated proteins

For identification of the protonated peptides, MS raw files of all runs were imported into the Progenesis QI LC-MS software (Nonlinear Dynamics, version 2.0), aligned globally, and analyzed simultaneously using the default parameter settings. MS/MS data were then exported directly from Progenesis in MGF format and searched using Mascot (Matrix Science, version 2.4.0) against a concatenated target-decoy *E. coli* protein database including forward and reversed sequences (UniProt, release date January 1, 2015, including 4479 target sequences). The search criteria were set as follows: 10 ppm precursor ion mass tolerance, 0.6-Da fragment ion mass tolerance, and full tryptic specificity required (cleavage after lysine or arginine residues); maximum three missed cleavages; fixed modification: carbamidomethylation (C), variable modification: oxidation (M). The database search results were filtered limiting the peptide and protein level false discovery rate (FDR) to 1%. The Mascot peptide identifications were subsequently imported into Progenesis and mapped to the detected MS1 peaks to ≤90%. The assigned MS1 peptide intensities were further processed using our in-house software script SafeQuant (55). This processing included normalization relative to the sum of all assigned MS1 peak intensities for individual LC-MS/MS runs and subsequent aggregation to protein abundances.

Quantification of deuterated proteins

An algorithm to analyze simultaneously both protonated and deuterated peptides within a single, mixed deuterated/protonated MS sample was developed using Python. The algorithm uses the protonated peptide positions identified by Progenesis as a starting point to search and quantitate both protonated and deuterated peptides within the two-dimensional retention time, m/z LC-MS data matrix. At first, the position and intensity of the mono-isotopic protonated peptide is redetermined by a local-maximum peak picker within a relative m/z tolerance of 3 ppm and the global retention time window given by Progenesis. The protonated peptide intensities determined by this algorithm correlated very well ($r^2 = 0.934$, $n = 4189$) with the corresponding Progenesis intensities (Fig. S3*A*). The correlation between the peptide intensities translated into an even stronger correlation between the protein intensities ($r^2 = 0.959$, $n = 1772$). Minor deviations are caused by using raw intensity data, not yet filtered for assigned proteins, differences in the sample alignment and peak detection of the two approaches, as well as the fact that only the modification by carbamidomethylation was taken into account in the Python routine.

Subsequently, the algorithm searches the corresponding heavy peptides within the same relative mass tolerance of 3 ppm and a shifted retention time window, which takes into account that the retention times of deuterated peptides are reduced because of their weaker RP-HPLC matrix interaction. The shifted window of the deuterated retention times RT_d was defined as $RT_p - \Delta t \leq RT_d < RT_p$, where RT_p is the protonated retention time and Δt defines the width of the window. The latter was determined using an iterative approach and set to 4

min based on the mean retention time shift of the deuterated relative to the protonated peptides (Fig. S4). Within this window, the five most abundant isotopologue peaks matching the predicted m/z values were identified by a local maximum search. These five peaks typically present ~99.5% of the theoretical isotopologue pattern, which was calculated using a binomial distribution and a conservative estimate of the residual protonation level of 1.5% based on deuterium labeling of individual medium components. The peak of the fully deuterated isotopologue typically had the highest intensity of all five and was subsequently used for quantification.

The heavy peptide intensities determined by our algorithm showed a high linear correlation ($r^2 = 0.825$, $n = 4189$) to the corresponding light intensities (Fig. S3*B*) translating again into an even higher correlation of the respective protein intensities ($r^2 = 0.859$, $n = 1772$). The fact that the majority of peptide abundances remained unchanged under deuteration agrees with the expectation that the change in the deuterated proteome is minor and validates the reliability of the deuterated peptide identification by the algorithm. As a negative control for the algorithm, the retention time window for the heavy peptide identification was shifted by 9 min, while retaining the same absolute window size (Fig. S3*C*). No correlation was obtained between the light and heavy peptide intensities ($r^2 = 0.023$, $n = 3965$). A further negative control on MS data acquired on a protonated peptide sample without admixture of deuterated peptides also yielded no correlation ($r^2 = 0.010$, $n = 1540$).

The linearity of protein abundance detection using this approach was assessed by analyzing 1:0.1, 1:0.33, 1:1, 0.33:1, and 0.1:1 mixtures of 0.5 μg/μl protonated and 0.5 μg/μl deuterated *E. coli* peptide solutions. MS1 intensities of all commonly identified protonated and deuterated peptides ($n = 4104$) from three LC-MS/MS analyses were summed separately and their ratio was compared with the ratio of protonated and deuterated input peptide concentrations (Fig. 3*A*). The data followed a linear dependence as MS(D)/MS(H) = 0.475 [D]/[H] ($r^2 = 0.9999$), where MS(D,H) presents the summed MS intensities of deuterated and protonated peptides, respectively, and [D]/[H] is the ratio of protonated and deuterated input peptide concentrations. The deviation of the proportionality factor 0.475 from unity is caused by the fact that only the highest intensity deuterated isotopologue peak was used in the summation, including the second highest intensity peak increases the proportionality factor to 0.898.

Following the identification and quantification of the individual peptides, the algorithm then combines the median values of the three most intense protonated and deuterated peptide intensities for a given protein to obtain total protein abundances for each condition and replicates thereof. The respective Python scripts are available upon request.

Analysis of the relative change in the protein abundance

To test for differential abundance, the empirical Bayes method (56) was applied and the obtained p values, which reflect the probability of detecting a given mean abundance difference across sample conditions by chance alone were corrected for multiple testing (q-values) using the Benjamini-Hochberg method (57).

For each condition, individual errors in the intensities were obtained from the standard deviation of triple biological replicates. A minimal error was imposed as 25% of the median of all intensity standard deviations of these replicates. The final errors in the relative protein abundances used for the COGs and GO analyses were derived by error propagation.

Clusters of orthologous groups of proteins annotations

COGs classifications were obtained from the COGs database (www.ncbi.nlm.nih.gov/COG, updated 2014).

Statistical analysis of Gene Ontology classes

Gene product annotations were obtained from the GO consortium database filtered for *E. coli* (www.geneontology.org, release date May 24, 2017, including 3545 genes)[3] (59, 60). The enrichment analysis was constrained to GO classes for which at least 75% of the associated protein abundances were detected by LC/MS. Proteins within these classes were categorized into strongly (at least 2-fold) up- or down-regulated and into not strongly (less than 2-fold) regulated based on their experimental variation. The statistical analysis was performed using Python 2.7.

Accession codes

All MS raw data files have been deposited to the ProteomeXchange Consortium via the PRIDE partner repository (58) with the data set identifier PXD009736.

Author contributions—C. O. and S. G. conceptualization; C. O., E. A., and A. S. software; C. O. and E. A. formal analysis; C. O., E. A., and K. N. G. investigation; C. O. visualization; C. O., E. A., K. N. G., and A. S. methodology; C. O. writing-original draft; C. O. and S. G. writing-review and editing; K. N. G. and A. S. resources; S. G. supervision; S. G. funding acquisition; S. G. project administration.

Acknowledgments—We gratefully acknowledge Drs. Alexia Loynton-Ferrand and Kai Schleicher from the Biozentrum Imaging Core Facility for expert help with light microscopy and Profs. Dirk Bumann, Erik van Nimwegen, and Henning Stahlberg for helpful discussions.

References

1. Katz, J. J., and Crespi, H. L. (1966) Deuterated organisms: Cultivation and uses. *Science* **151,** 1187–1194 CrossRef Medline
2. Brooks, S. C. (1937) Osmotic effects of deuterium oxide (heavy water) on living cells. *Science* **86,** 497–498 CrossRef Medline
3. Chance, H. L., and Allen, W. C. (1946) Influence of heavy water on growth, morphology, and fermentation reactions of *Eberthella typhosa*. *J. Bacteriol.* **51,** 547–551 Medline
4. Flaumenhaft, E., Bose, S., Crespi, H. L., and Katz, J. J. (1965) Deuterium isotope effects in cytology. *Int. Rev. Cytol.* **18,** 313–361 CrossRef Medline
5. Evans, B. R., and Shah, R. (2015) Development of approaches for deuterium incorporation in plants. *Methods Enzymol.* **565,** 213–243 CrossRef Medline
6. Urey, H. C., Brickwedde, F. G., and Murphy, G. M. (1932) A hydrogen isotope of mass 2. *Phys. Rev.* **39,** 164 CrossRef

[3] Please note that the JBC is not responsible for the long-term archiving and maintenance of this site or any other third party hosted site.

7. Unno, K., Busujima, H., Shimba, S., Narita, K., and Okada, S. (1988) Characteristics of growth and deuterium incorporation in *Chlorella ellipsoidea* grown in deuterium oxide. *Chem. Pharm. Bull.* **36,** 1828–1833 CrossRef
8. Kuchitsu, K., and Bartell, L. S. (1962) Effect of anharmonic vibrations on the bond lengths of polyatomic molecules. II. Cubic constants and equilibrium bond lengths of methane. *J. Chem. Phys.* **36,** 2470–2481 CrossRef
9. Steiner, T., and Saenger, W. (1994) Lengthening of the covalent O–H bond in O–H . . . O hydrogen bonds re-examined from low-temperature neutron diffraction data of organic compounds. *Acta Crystallogr B.* **50,** 348–357 CrossRef
10. Mugridge, J. S., Bergman, R. G., and Raymond, K. N. (2010) Does size really matter? The steric isotope effect in a supramolecular host-guest exchange reaction. *Angew. Chem. Int. Ed. Engl.* **49,** 3635–3637 CrossRef Medline
11. Haynes, W. M. (ed) (2009) *CRC Handbook of Chemistry and Physics*, CRC Press, Boca Raton, FL
12. Krezel, A., and Bal, W. (2004) A formula for correlating pKa values determined in D2O and H_2O. *J. Inorg. Biochem.* **98,** 161–166 CrossRef Medline
13. Ubbelohde, A. R., and Gallagher, K. J. (1955) Acid-base effects in hydrogen bonds in crystals. *Acta Crystallogr.* **8,** 71–83 CrossRef
14. Jaravine, V. A., Cordier, F., and Grzesiek, S. (2004) Quantification of H/D isotope effects on protein hydrogen-bonds by h3JNC′ and 1JNC′ couplings and peptide group 15N and 13C′ chemical shifts. *J. Biomol. NMR* **29,** 309–318 CrossRef Medline
15. Westheimer, F. H. (1961) The magnitude of the primary kinetic isotope effect for compounds of hydrogen and deuterium. *Chem. Rev.* **61,** 265–273 CrossRef
16. Knapp, M. J., Rickert, K., and Klinman, J. P. (2002) Temperature-dependent isotope effects in soybean lipoxygenase-1: Correlating hydrogen tunneling with protein dynamics. *J. Am. Chem. Soc.* **124,** 3865–3874 CrossRef Medline
17. Layfield, J. P., and Hammes-Schiffer, S. (2014) Hydrogen tunneling in enzymes and biomimetic models. *Chem. Rev.* **114,** 3466–3494 CrossRef Medline
18. Izzo, V., Fornili, S. L., and Cordone, L. (1975) Thermal denaturation of *B. subtilis* DNA in H_2O and D_2O observed by electron microscopy. *Nucleic Acids Res.* **2,** 1805–1810 CrossRef Medline
19. Cupane, A., Vitrano, E., San Biago, P. L., Madonia, F., and Palma, M. U. (1980) Thermal stability of poly(A) and poly(U) complexes in H_2O and D_2O: Isotopic effects on critical temperatures and transition widths. *Nucleic Acids Res.* **8,** 4283–4303 CrossRef Medline
20. Beranová, L., Humpolíčková, J., Sýkora, J., Benda, A., Cwiklik, L., Jurkiewicz, P., Gröbner, G., and Hof, M. (2012) Effect of heavy water on phospholipid membranes: Experimental confirmation of molecular dynamics simulations. *Phys. Chem. Chem. Phys.* **14,** 14516–14522 CrossRef Medline
21. Hattori, A., Crespi, H. L., and Katz, J. J. (1965) Effect of side-chain deuteration on protein stability. *Biochemistry* **4,** 1213–1225 CrossRef Medline
22. Antonino, L. C., Kautz, R. A., Nakano, T., Fox, R. O., and Fink, A. L. (1991) Cold denaturation and 2H2O stabilization of a staphylococcal nuclease mutant. *Proc. Natl. Acad. Sci. U.S.A.* **88,** 7715–7718 CrossRef Medline
23. Makhatadze, G. I., Clore, G. M., and Gronenborn, A. M. (1995) Solvent isotope effect and protein stability. *Nat. Struct. Mol. Biol.* **2,** 852–855 CrossRef Medline
24. Guzzi, R., Sportelli, L., La Rosa, C., Milardi, D., and Grasso, D. (1998) Solvent isotope effects on azurin thermal unfolding. *J. Phys. Chem. B.* **102,** 1021–1028 CrossRef
25. Kuhlman, B., and Raleigh, D. P. (1998) Global analysis of the thermal and chemical denaturation of the N-terminal domain of the ribosomal protein L9 in H_2O and D_2O. Determination of the thermodynamic parameters, $\Delta H°$, $\Delta S°$, and $\Delta C°p$, and evaluation of solvent isotope effects. *Protein Sci.* **7,** 2405–2412 CrossRef Medline
26. Huyghues-Despointes, B. M. P., Scholtz, J. M., and Pace, C. N. (1999) Protein conformational stabilities can be determined from hydrogen exchange rates. *Nat. Struct. Mol. Biol.* **6,** 910–912 CrossRef
27. Chellgren, B. W., and Creamer, T. P. (2004) Effects of H_2O and D_2O on polyproline II helical structure. *J. Am. Chem. Soc.* **126,** 14734–14735 CrossRef Medline
28. Cho, Y., Sagle, L. B., Iimura, S., Zhang, Y., Kherb, J., Chilkoti, A., Scholtz, J. M., and Cremer, P. S. (2009) Hydrogen bonding of β-turn structure is stabilized in D_2O. *J. Am. Chem. Soc.* **131,** 15188–15193 CrossRef Medline
29. Piszczek, G., Lee, J. C., Tjandra, N., Lee, C.-R., Seok, Y.-J., Levine, R. L., and Peterkofsky, A. (2011) Deuteration of *Escherichia coli* enzyme INtr alters its stability. *Arch. Biochem. Biophys.* **507,** 332–342 CrossRef Medline
30. Knoll, W. (1981) Volume determination of deuterated dimyristoyllecithin by mass and scattering length densitometry. *Chem. Phys. Lipids* **28,** 337–345 CrossRef
31. Guard-Friar, D., Chen, C. H., and Engle, A. S. (1985) Deuterium isotope effect on the stability of molecules: Phospholipids. *J. Phys. Chem.* **89,** 1810–1813 CrossRef
32. Gross, P. R., and Spindel, W. (1960) Mitotic arrest by deuterium oxide. *Science* **131,** 37–38 CrossRef Medline
33. Lamprecht, J., Schroeter, D., and Paweletz, N. (1991) Derangement of microtubule arrays in interphase and mitotic PtK2 cells treated with deuterium oxide (heavy water). *J. Cell Sci.* **98**, 463–473 Medline
34. Panda, D., Chakrabarti, G., Hudson, J., Pigg, K., Miller, H. P., Wilson, L., and Himes, R. H. (2000) Suppression of microtubule dynamic instability and treadmilling by deuterium oxide. *Biochemistry* **39,** 5075–5081 CrossRef Medline
35. Hohlefelder, L. S., Stögbauer, T., Opitz, M., Bayerl, T. M., and Rädler, J. O. (2013) Heavy water reduces GFP expression in prokaryotic cell-free assays at the translation level while stimulating its transcription. *Biomed Res. Int.* **2013,** 1–9 CrossRef Medline
36. Hochuli, M., Szyperski, T., and Wüthrich, K. (2000) Deuterium isotope effects on the central carbon metabolism of *Escherichia coli* cells grown on a D2O-containing minimal medium. *J. Biomol. NMR* **17,** 33–42 CrossRef Medline
37. Schmidt, A., Kochanowski, K., Vedelaar, S., Ahrne, E., Volkmer, B., Callipo, L., Knoops, K., Bauer, M., Aebersold, R., and Heinemann, M. (2015) The quantitative and condition-dependent *Escherichia coli* proteome. *Nat. Biotechnol.* **34,** 104–110 CrossRef Medline
38. Wiśniewski, J. R., Hein, M. Y., Cox, J., and Mann, M. (2014) A "proteomic ruler" for protein copy number and concentration estimation without spike-in standards. *Mol. Cell. Proteomics* **13,** 3497–3506 CrossRef Medline
39. Tatusov, R. L., Fedorova, N. D., Jackson, J. D., Jacobs, A. R., Kiryutin, B., Koonin, E. V., Krylov, D. M., Mazumder, R., Mekhedov, S. L., Nikolskaya, A. N., Rao, B. S., Smirnov, S., Sverdlov, A. V., Vasudevan, S., Wolf, Y. I., Yin, J. J., and Natale, D. A. (2003) The COG database: An updated version includes eukaryotes. *BMC Bioinformatics* **4,** 41 CrossRef Medline
40. Scott, M., Klumpp, S., Mateescu, E. M., and Hwa, T. (2014) Emergence of robust growth laws from optimal regulation of ribosome synthesis. *Mol. Syst. Biol.* **10,** 747–747 CrossRef Medline
41. Olson, E. R., Dunyak, D. S., Jurss, L. M., and Poorman, R. A. (1991) Identification and characterization of dppA, an *Escherichia coli* gene encoding a periplasmic dipeptide transport protein. *J. Bacteriol.* **173,** 234–244 CrossRef Medline
42. Park, S. J., McCabe, J., Turna, J., and Gunsalus, R. P. (1994) Regulation of the citrate synthase (gltA) gene of *Escherichia coli* in response to anaerobiosis and carbon supply: Role of the arcA gene product. *J. Bacteriol.* **176,** 5086–5092 CrossRef Medline
43. Wolfe, A. J. (2005) The acetate switch. *Microbiol. Mol. Biol. Rev.* **69,** 12–50 CrossRef Medline
44. Lee, J., Hiibel, S. R., Reardon, K. F., and Wood, T. K. (2009) Identification of stress-related proteins in *Escherichia coli* using the pollutant *cis*-dichloroethylene. *J. Appl. Microbiol.* **108,** 2088–2102 CrossRef Medline
45. Zhang, X.-S., Garcia-Contreras, R., and Wood, T. K. (2007) YcfR (BhsA) influences *Escherichia coli* biofilm formation through stress response and surface hydrophobicity. *J. Bacteriol.* **189,** 3051–3062 CrossRef Medline
46. Jackson, D. W., Simecka, J. W., and Romeo, T. (2002) Catabolite repression of *Escherichia coli* biofilm formation. *J. Bacteriol.* **184,** 3406–3410 CrossRef Medline
47. Farver, O., Zhang, J., Chi, Q., Pecht, I., and Ulstrup, J. (2001) Deuterium isotope effect on the intramolecular electron transfer in *Pseudomonas aeruginosa* azurin. *Proc. Natl. Acad. Sci. U.S.A.* **98,** 4426–4430 CrossRef Medline

48. Ranieri, A., Battistuzzi, G., Borsari, M., Bortolotti, C. A., Di Rocco, G., and Sola, M. (2012) pH and solvent H/D Isotope effects on the thermodynamics and kinetics of electron transfer for electrode-immobilized native and urea-unfolded stellacyanin. *Langmuir* **28,** 15087–15094 CrossRef Medline
49. Dassain, M., Leroy, A., Colosetti, L., Carolé, S., and Bouché, J.-P. (1999) A new essential gene of the 'minimal genome' affecting cell division. *Biochimie* **81,** 889–895 CrossRef Medline
50. Lamprecht, J., Schroeter, D., and Paweletz, N. (1989) Disorganization of mitosis in HeLa cells by deuterium oxide. *Eur. J. Cell Biol.* **50,** 360–369 Medline
51. Schroeter, D., Lamprecht, J., Eckhardt, R., Futterman, G., and Paweletz, N. (1992) Deuterium oxide (heavy water) arrests the cell cycle of PtK2 cells during interphase. *Eur. J. Cell Biol.* **58,** 365–370 Medline
52. Daegelen, P., Studier, F. W., Lenski, R. E., Cure, S., and Kim, J. F. (2009) Tracing ancestors and relatives of *Escherichia coli* B, and the derivation of B strains REL606 and BL21(DE3). *J. Mol. Biol.* **394,** 634–643 CrossRef Medline
53. Sommer, C., Strähle, C. N., Köthe, U., and Hamprecht, F. A. (2011) ilastik: Interactive learning and segmentation toolkit. in *2011 IEEE International Symposium on Biomedical Imaging: From Nano to Macro, March 30–April 2, 2011*, pp. 230–233, IEEE Operations Centers, Piscataway, NJ CrossRef
54. Carpenter, A. E., Jones, T. R., Lamprecht, M. R., Clarke, C., Kang, I. H., Friman, O., Guertin, D. A., Chang, J. H., Lindquist, R. A., Moffat, J., Golland, P., and Sabatini, D. M. (2006) CellProfiler: Image analysis software for identifying and quantifying cell phenotypes. *Genome Biol.* **7,** R100 CrossRef Medline
55. Glatter, T., Ludwig, C., Ahrné, E., Aebersold, R., Heck, A. J. R., and Schmidt, A. (2012) Large-scale quantitative assessment of different in-solution protein digestion protocols reveals superior cleavage efficiency of tandem Lys-C/Trypsin proteolysis over trypsin digestion. *J. Proteome Res.* **11,** 5145–5156 CrossRef Medline
56. Smyth, G. K. (2004) Linear models and empirical Bayes methods for assessing differential expression in microarray experiments. *Stat. Appl. Genet. Mol. Biol.* **3,** Article 3 CrossRef Medline
57. Benjamini, Y., and Hochberg, Y. (1995) Controlling the false discovery rate: A practical and powerful approach to multiple testing. *J. R. Stat. Soc. Series B Stat. Methodol.* **57,** 289–300
58. Vizcaíno, J. A., Côté, R. G., Csordas, A., Dianes, J. A., Fabregat, A., Foster, J. M., Griss, J., Alpi, E., Birim, M., Contell, J., O'Kelly, G., Schoenegger, A., Ovelleiro, D., Pérez-Riverol, Y., Reisinger, F., Ríos, D., Wang, R., and Hermjakob, H. (2013) The Proteomics Identifications (PRIDE) database and associated tools: Status in 2013. *Nucleic Acids Res.* **41,** D1063–D1069 CrossRef Medline
59. Ashburner, M., Ball, C. A., Blake, J. A., Botstein, D., Butler, H., Cherry, J. M., Davis, A. P., Dolinski, K., Dwight, S. S., Eppig, J. T., Harris, M. A., Hill, D. P., Issel-Tarver, L., Kasarskis, A., Lewis, S., Matese, J. C., Richardson, J. E., Ringwald, M., Rubin, G. M., Sherlock, G. (2000) Gene ontology: Tool for the unification of biology. The Gene Ontology Consortium. *Nat. Genet.* **25,** 25–29 CrossRef Medline
60. The Gene Ontology Consortium (2017) Expansion of the Gene Ontology knowledgebase and resources. *Nucleic Acids Res.* **45,** D331–D338 CrossRef Medline

Deuterium induces a distinctive *Escherichia coli* proteome that correlates with the reduction in growth rate

Christian Opitz, Erik Ahrné, Kenneth N. Goldie, Alexander Schmidt and Stephan Grzesiek

J. Biol. Chem. 2019, 294:2279-2292.
doi: 10.1074/jbc.RA118.006914 originally published online December 13, 2018

Deuterium induces a distinctive proteome in *Escherichia coli*

Christian Opitz[1], Erik Ahrné[1], Kenneth N. Goldie[2], Alexander Schmidt[1] and Stephan Grzesiek[1]*

[1]Biozentrum, University of Basel, CH-4056 Basel, Switzerland

[2]Center for Cellular Imaging and Nanoanalytics, Biozentrum, University of Basel, CH-4058 Basel, Switzerland

Supporting Information

*Address correspondence to:
Stephan Grzesiek
Focal Area Structural Biology and Biophysics, Biozentrum
University of Basel, CH-4056 Basel, Switzerland
Phone: ++41 61 267 2100
FAX: ++41 61 267 2109
Email: Stephan.Grzesiek@unibas.ch

Figure legends

Figure S1. Complete set of significantly regulated Gene ontology (GO) classes for proteomes obtained from *E. coli* cells exponentially grown in protonated M9 minimal (M9H3e) vs. protonated full (LBe) medium. The analysis is reduced to (GO classes, for which ≥75% of the contained proteins (total number N_{tot}) were observed with such low variation that they could be classified as either strongly (at least two-fold) up-regulated (number N_{up}), strongly (at least two-fold) down-regulated (number N_{down}), or as not strongly regulated (less than two-fold, number $N_{not\text{-}regulated}$). An entire GO class is considered as strongly up- (red) or downregulated (blue) when ≥50% of its significantly detected proteins ($N_{up} + N_{not\text{-}regulated} + N_{down}$) are at least two-fold up- or downregulated, respectively. Several clusters (magenta) also showed significant combined up- and down-regulation [$(N_{up} + N_{down})/(N_{up} + N_{not\text{-}regulated} + N_{down}) \geq 50\%$] of their detected proteins, albeit they were not significantly regulated in one direction (up or down). The values in the last line of each GO class indicate from left to right: the number of significantly up-regulated N_{up}, significantly not-regulated $N_{not\text{-}regulated}$, significantly down-regulated N_{down}, not significantly detected $N_{not\text{-}significant}$, as well as the total number of proteins in the class N_{tot}.

Figure S2. Complete set of regulated Gene ontology (GO) classes for proteomes obtained from *E. coli* cells exponentially grown in deuterated M9 minimal (M9D3e) vs. protonated M9 minimal (M9H3e) medium. The analysis, color coding and annotation are identical to the comparison of protonated M9 minimal (M9H3e) vs. protonated full (LBe) medium shown in Figure S1.

Figure S3. Validation of algorithm for the identification of protonated and deuterated peptides in LC/MS data. **a** Correlation of normalized protonated (light) peptide intensities identified using the in-house peak detection algorithm and the *Progenesis* software package. **b** Correlation of normalized protonated (light) and related deuterated (heavy) peptide intensities identified using the developed algorithm. **c** Negative control of heavy peptide identification using a retention time window shifted by 9 minutes relative to the expected heavy peptide retention time. The plot shows the correlation between the normalized light and the (erroneously) identified heavy peptide intensities. The color-coding in each panel gives the point density in arbitrary units (right bar), whereas the dashed black line indicates the diagonal. A detailed description of the applied algorithm is given in the Method section.

Figure S4. Histogram of mean retention time shifts (Δt) of deuterated peptides relative to protonated peptides. Retentions times were determined simultaneously for a sample containing protonated and deuterated peptides in a 1:1 ratio (see Methods).

ribonucleoprotein complex GO:1990904 [+0, 45, -0, 12] 58
oxidoreductase activity, acting on a sulfur group of donors, disulfide as acceptor GO:0016671 [+1, 6, -0, 1] 9
protein transport by the Tat complex GO:0043953 [+0, 3, -0, 1] 4
nucleotide phosphorylation GO:0046939 [+2, 10, -0, 1] 14
nucleoside diphosphate metabolic process GO:0009132 [+2, 12, -0, 2] 18
nucleoside triphosphate metabolic process GO:0009141 [+2, 14, -1, 3] 22
glycosyl compound biosynthetic process GO:1901659 [+1, 4, -4, 2] 12
thiosulfate sulfurtransferase activity GO:0004792 [+1, 2, -0, 1] 4
ligase activity, forming carbon-oxygen bonds GO:0016875 [+0, 15, -0, 4] 19
hydroxymethyl-, formyl- and related transferase activity GO:0016742 [+2, 3, -0, 1] 6
alditol metabolic process GO:0019400 [+2, 3, -2, 1] 8
keto-3-deoxy-D-manno-octulosonic acid metabolic process GO:0046400 [+0, 3, -0, 1] 4
pyridoxal 5'-phosphate salvage GO:0009443 [+0, 2, -1, 0] 3
intracellular ribonucleoprotein complex GO:0030529 [+0, 45, -0, 12] 58
hydroperoxide reductase activity GO:0032843 [+0, 3, -0, 1] 4
nucleoside diphosphate phosphorylation GO:0006165 [+2, 10, -0, 1] 14
purine nucleoside diphosphate metabolic process GO:0009135 [+2, 12, -0, 1] 17
ribonucleoside diphosphate metabolic process GO:0009185 [+2, 12, -0, 1] 17
purine nucleoside monophosphate metabolic process GO:0009126 [+2, 14, -2, 3] 23
nucleoside triphosphate biosynthetic process GO:0009142 [+0, 2, -1, 1] 4
ribonucleoside triphosphate metabolic process GO:0009199 [+2, 13, -1, 2] 20
purine nucleoside triphosphate metabolic process GO:0009144 [+2, 13, -0, 2] 19
nucleoside biosynthetic process GO:0009163 [+1, 4, -4, 2] 12
keto-3-deoxy-D-manno-octulosonic acid biosynthetic process GO:0019294 [+0, 3, -0, 1] 4
NADH dehydrogenase complex GO:0030964 [+0, 10, -1, 2] 14
ligase activity, forming aminoacyl-tRNA and related compounds GO:0016876 [+0, 15, -0, 4] 19
glycerol metabolic process GO:0006071 [+0, 2, -2, 0] 4
alditol catabolic process GO:0019405 [+2, 2, -2, 1] 7
hexitol metabolic process GO:0006059 [+2, 1, -0, 1] 4
ribosome GO:0005840 [+0, 44, -0, 12] 57
racemase and epimerase activity, acting on amino acids and derivatives GO:0016855 [+0, 3, -0, 1] 4
purine ribonucleoside diphosphate metabolic process GO:0009179 [+2, 12, -0, 1] 17
purine ribonucleoside monophosphate metabolic process GO:0009167 [+2, 14, -2, 3] 23
ribonucleoside triphosphate biosynthetic process GO:0009201 [+0, 2, -1, 0] 3
purine ribonucleoside triphosphate metabolic process GO:0009205 [+2, 13, -0, 2] 19
pyrimidine nucleoside biosynthetic process GO:0046134 [+0, 1, -1, 0] 2
aminoacyl-tRNA ligase activity GO:0004812 [+0, 15, -0, 4] 19
glycerol catabolic process GO:0019563 [+0, 1, -2, 0] 3
hexitol catabolic process GO:0019407 [+2, 1, -0, 1] 4
oxidoreductase activity, oxidizing metal ions GO:0016722 [+1, 2, -1, 0] 4
lipoprotein localization GO:0044872 [+0, 4, -0, 1] 5
respiratory chain complex I GO:0045271 [+0, 10, -0, 2] 13
cytosolic ribosome GO:0022626 [+0, 44, -0, 11] 56
ribosomal subunit GO:0044391 [+0, 44, -0, 11] 56
protein folding GO:0006457 [+3, 18, -0, 2] 28
ADP metabolic process GO:0046031 [+2, 12, -0, 1] 17
ATP metabolic process GO:0046034 [+2, 13, -0, 1] 18
ATP generation from ADP GO:0006757 [+2, 10, -0, 1] 14
isopentenyl diphosphate metabolic process GO:0046490 [+0, 3, -0, 1] 4
amino acid activation GO:0043038 [+0, 17, -0, 5] 22
RNA polymerase binding GO:0070063 [+0, 3, -2, 1] 6
carbon-oxygen lyase activity, acting on phosphates GO:0016838 [+1, 2, -0, 1] 4
anaerobic glycerol catabolic process GO:0019588 [+0, 1, -1, 0] 2
mRNA binding GO:0003729 [+0, 10, -1, 2] 13
oxidoreductase activity, oxidizing metal ions, oxygen as acceptor GO:0016724 [+0, 2, -1, 0] 3
lipoprotein localization to membrane GO:0044873 [+0, 4, -0, 1] 5
plasma membrane respiratory chain complex I GO:0045272 [+0, 10, -0, 2] 13
small ribosomal subunit GO:0015935 [+0, 18, -0, 5] 24
large ribosomal subunit GO:0015934 [+0, 26, -0, 6] 32
chaperone-mediated protein folding GO:0061077 [+2, 14, -0, 1] 20
protein refolding GO:0042026 [+0, 5, -0, 1] 6
proton-transporting two-sector ATPase complex GO:0016469 [+0, 6, -0, 2] 8
isopentenyl diphosphate biosynthetic process GO:0009240 [+0, 3, -0, 1] 4
tRNA aminoacylation GO:0043039 [+0, 17, -0, 4] 21
RNA polymerase core enzyme binding GO:0043175 [+0, 3, -2, 1] 6
vitamin B6 metabolic process GO:0042816 [+1, 5, -1, 2] 9
NADH dehydrogenase (quinone) activity GO:0050136 [+0, 5, -1, 0] 7
ornithine metabolic process GO:0006591 [+1, 2, -0, 0] 3
ferroxidase activity GO:0004322 [+0, 2, -1, 0] 3
lipoprotein localization to outer membrane GO:0044874 [+0, 4, -0, 1] 5
fatty acid binding GO:0005504 [+1, 2, -0, 1] 4
cytosolic small ribosomal subunit GO:0022627 [+0, 18, -0, 5] 24
cytosolic large ribosomal subunit GO:0022625 [+0, 26, -0, 6] 32
D-amino acid transport GO:0042940 [+1, 2, -0, 1] 4
N2-acetyl-L-ornithine:2-oxoglutarate 5-aminotransferase activity GO:0003992 [+1, 2, -0, 0] 3
glycolytic process GO:0006096 [+2, 9, -0, 1] 13
proton-transporting ATP synthase complex GO:0045259 [+0, 6, -0, 2] 8
isopentenyl diphosphate biosynthetic process, methylerythritol 4-phosphate pathway GO:0019288 [+0, 3, -0, 1] 4
tRNA aminoacylation for protein translation GO:0006418 [+0, 17, -0, 4] 21
bacterial-type RNA polymerase core enzyme binding GO:0001000 [+0, 2, -1, 1] 4
nucleobase-containing compound kinase activity GO:0019205 [+1, 3, -3, 1] 9
queuosine metabolic process GO:0046116 [+1, 2, -2, 0] 6
transcription antitermination GO:0031564 [+0, 6, -0, 2] 8
oxidoreductase activity, acting on NAD(P)H, nitrogenous group as acceptor GO:0016657 [+0, 2, -1, 0] 4
ATPase activity, coupled to transmembrane movement of ions, rotational mechanism GO:0044769 [+0, 6, -0, 2] 8
D-methionine transport GO:0048473 [+1, 2, -0, 0] 3
secondary metabolite catabolic process GO:0090487 [+1, 2, -0, 0] 4
fatty acid synthase activity GO:0004312 [+0, 4, -0, 1] 5
phosphofructokinase activity GO:0008443 [+0, 2, -1, 0] 3
'de novo' pyrimidine nucleobase biosynthetic process GO:0006207 [+0, 4, -0, 1] 5
protein disulfide oxidoreductase activity GO:0015035 [+0, 8, -0, 1] 10
modified amino acid binding GO:0072341 [+1, 3, -0, 1] 5
uridylyltransferase activity GO:0070569 [+0, 3, -1, 0] 5
TAT protein transport complex GO:0033281 [+0, 3, -0, 1] 4
translation regulator activity, nucleic acid binding GO:0090079 [+0, 3, -0, 1] 4
endoribonuclease activity, producing 5'-phosphomonoesters GO:0016891 [+0, 2, -1, 0] 4
nucleotide kinase activity GO:0019201 [+0, 3, -2, 1] 6
queuosine biosynthetic process GO:0008616 [+1, 2, -2, 0] 6
peroxiredoxin activity GO:0051920 [+1, 2, -0, 1] 4
proline metabolic process GO:0006560 [+0, 3, -0, 1] 4
protein unfolding GO:0043335 [+0, 3, -0, 1] 4
protein stabilization GO:0050821 [+1, 3, -0, 1] 5
ubiquinone binding GO:0048039 [+0, 3, -1, 1] 5
response to cadmium ion GO:0046686 [+1, 1, -1, 1] 4
response to hydroperoxide GO:0033194 [+1, 3, -0, 0] 4
rRNA binding GO:0019843 [+0, 18, -2, 6] 26
regulation of lipid metabolic process GO:0019216 [+0, 3, -0, 1] 4
ferric iron binding GO:0008199 [+0, 2, -1, 1] 4
purine nucleotide interconversion GO:0015950 [+0, 2, -1, 0] 3
selenocysteine metabolic process GO:0016259 [+0, 3, -0, 1] 4
aldehyde biosynthetic process GO:0046184 [+1, 4, -1, 2] 8
amino acid kinase activity GO:0019202 [+3, 2, -0, 0] 6
phosphotransferase activity, carboxyl group as acceptor GO:0016774 [+3, 4, -1, 0] 10
monosaccharide transmembrane transport GO:1905950 [+2, 1, -0, 1] 4
cellular response to radiation GO:0071478 [+1, 1, -0, 0] 2
one-carbon metabolic process GO:0006730 [+1, 1, -0, 0] 2
cyclohydrolase activity GO:0019238 [+2, 1, -1, 0] 4
indole-containing compound metabolic process GO:0042430 [+5, 1, -0, 0] 6
iron assimilation GO:0033212 [+4, 1, -0, 0] 5
aspartate kinase activity GO:0004072 [+2, 1, -0, 0] 4
hexose transmembrane transport GO:0035428 [+2, 1, -0, 1] 4
cellular response to light stimulus GO:0071482 [+1, 1, -0, 0] 2
tetrahydrofolate interconversion GO:0035999 [+1, 1, -0, 0] 2
GTP cyclohydrolase activity GO:0003933 [+1, 0, -1, 0] 2
imidazole-containing compound metabolic process GO:0052803 [+7, 0, -0, 1] 8
cellular amino acid biosynthetic process GO:0008652 [+49, 18, -1, 12] 88
aromatic amino acid family metabolic process GO:0009072 [+11, 1, -0, 1] 13
indolalkylamine metabolic process GO:0006586 [+5, 1, -0, 0] 6
iron assimilation by chelation and transport GO:0033214 [+1, 1, -0, 0] 2
glucose transmembrane transport GO:1904659 [+2, 1, -0, 1] 4
carbohydrate import across plasma membrane GO:0098704 [+2, 1, -0, 1] 4
cellular response to UV GO:0034644 [+1, 1, -0, 0] 2
histidine metabolic process GO:0006547 [+7, 0, -0, 1] 8
branched-chain amino acid biosynthetic process GO:0009082 [+12, 1, -0, 2] 16
valine metabolic process GO:0006573 [+7, 2, -0, 2] 12
alpha-amino acid biosynthetic process GO:1901607 [+45, 17, -1, 9] 79
erythrose 4-phosphate/phosphoenolpyruvate family amino acid metabolic process GO:1902221 [+3, 0, -0, 1] 4
aromatic amino acid family biosynthetic process GO:0009073 [+11, 0, -0, 1] 12
tryptophan metabolic process GO:0006568 [+5, 1, -0, 0] 6
transferase activity, transferring aldehyde or ketonic groups GO:0016744 [+5, 3, -0, 1] 10
glucose import across plasma membrane GO:0098708 [+2, 1, -0, 1] 4
histidine biosynthetic process GO:0000105 [+7, 0, -0, 1] 8
valine biosynthetic process GO:0009099 [+7, 1, -0, 0] 9
aspartate family amino acid biosynthetic process GO:0009067 [+12, 4, -0, 2] 21
homoserine metabolic process GO:0009092 [+3, 1, -0, 0] 4
serine family amino acid biosynthetic process GO:0009070 [+8, 6, -1, 1] 17
L-serine metabolic process GO:0006563 [+5, 2, -3, 0] 11
glutamine family amino acid biosynthetic process GO:0009084 [+3, 8, -0, 3] 14
erythrose 4-phosphate/phosphoenolpyruvate family amino acid biosynthetic process GO:1902223 [+3, 0, -0, 1] 4
aromatic amino acid family biosynthetic process, prephenate pathway GO:0009095 [+3, 0, -0, 1] 4
L-phenylalanine metabolic process GO:0006558 [+3, 0, -0, 1] 4
lactate oxidation GO:0019516 [+1, 1, -0, 0] 2
5-methyltetrahydrofolate-dependent methyltransferase activity GO:0042084 [+1, 1, -0, 0] 2
methionine transport GO:0015821 [+2, 2, -0, 0] 5
polyamine binding GO:0019808 [+1, 1, -0, 0] 2
ammonium ion binding GO:0070405 [+1, 1, -0, 0] 2
P-P-bond-hydrolysis-driven protein transmembrane transporter activity GO:0015450 [+3, 4, -0, 1] 8
lysine biosynthetic process GO:0009085 [+5, 2, -0, 1] 9
homoserine biosynthetic process GO:0009090 [+3, 1, -0, 0] 4
glycine biosynthetic process GO:0006545 [+1, 1, -0, 0] 2
cysteine biosynthetic process GO:0019344 [+2, 1, -0, 0] 4
L-serine biosynthetic process GO:0006564 [+2, 1, -1, 0] 4
L-serine catabolic process GO:0006565 [+1, 0, -2, 0] 4
arginine biosynthetic process GO:0006526 [+1, 5, -0, 2] 8
L-phenylalanine biosynthetic process GO:0009094 [+3, 0, -0, 1] 4
homocysteine metabolic process GO:0050667 [+1, 1, -0, 0] 2
ligand-gated channel activity GO:0022834 [+1, 0, -1, 0] 2
methionine synthase activity GO:0008705 [+1, 1, -0, 0] 2
D-methionine transport GO:0048473 [+1, 2, -0, 0] 3
putrescine binding GO:0019810 [+1, 1, -0, 0] 2
bacteriocin transmembrane transporter activity GO:0022885 [+2, 1, -0, 0] 3
proton motive force dependent protein transmembrane transporter activity GO:0009977 [+1, 2, -0, 1] 4
acetate metabolic process GO:0006083 [+1, 1, -2, 0] 5
cysteine biosynthetic process from serine GO:0006535 [+2, 1, -0, 0] 3
arginine biosynthetic process via ornithine GO:0042450 [+1, 2, -0, 0] 3
L-isoleucine transmembrane transporter activity GO:0015188 [+3, 0, -1, 0] 5
protein-N(PI)-phosphohistidine-sugar phosphotransferase activity GO:0008982 [+2, 0, -1, 1] 4
asparagine metabolic process GO:0006528 [+2, 1, -0, 0] 3
cysteine synthase complex GO:0009333 [+1, 1, -0, 0] 2
colicin transmembrane transporter activity GO:0042912 [+2, 1, -0, 0] 3
lysine biosynthetic process via diaminopimelate and N-succinyl-2-amino-6-ketopimelate GO:0033359 [+1, 1, -0, 0] 2
acetate catabolic process GO:0045733 [+1, 0, -1, 0] 2
homoserine dehydrogenase activity GO:0004412 [+1, 1, -0, 0] 2
fructose import GO:0032445 [+2, 0, -2, 1] 5
polyol transport GO:0015791 [+3, 1, -1, 1] 6
phosphotransferase activity, paired acceptors GO:0016781 [+1, 1, -0, 0] 2
oligopeptide binding GO:1900750 [+1, 1, -0, 0] 2
cadmium ion binding GO:0046870 [+1, 0, -1, 0] 2
4-aminobutyrate transaminase activity GO:0003867 [+1, 1, -0, 0] 2
response to oxygen radical GO:0000305 [+0, 2, -1, 0] 3
pyridoxal kinase activity GO:0008478 [+0, 1, -1, 0] 2
amino sugar biosynthetic process GO:0046349 [+0, 2, -2, 1] 5
UDP-N-acetylglucosamine metabolic process GO:0006047 [+0, 1, -2, 1] 4
DNA packaging complex GO:0044815 [+0, 1, -1, 0] 2
RNA binding transcription factor activity GO:0001070 [+0, 2, -2, 0] 4
maintenance of location GO:0051235 [+0, 1, -1, 0] 2
adenosine metabolic process GO:0046085 [+0, 1, -1, 0] 2
negative regulation of protein complex disassembly GO:0043242 [+0, 1, -2, 0] 3
lipoate-protein ligase activity GO:0016979 [+0, 1, -1, 0] 2
transferase activity, transferring alkylthio groups GO:0050497 [+0, 1, -1, 0] 2
purine-containing compound salvage GO:0043101 [+0, 1, -2, 1] 4
protein lipoylation GO:0009249 [+0, 1, -1, 0] 2
fatty acid transport GO:0015908 [+0, 1, -1, 0] 2
non-glycolytic fermentation GO:0019662 [+0, 1, -1, 0] 2
proline transport GO:0015824 [+0, 1, -1, 0] 2
methylglyoxal reductase (NADPH-dependent, acetol producing) GO:1990002 [+0, 1, -1, 0] 2
L-proline transmembrane transporter activity GO:0015193 [+0, 1, -1, 0] 2
fructose metabolic process GO:0006000 [+0, 1, -1, 0] 2
translation initiation factor activity GO:0003743 [+0, 1, -1, 0] 2
cellular response to oxygen radical GO:0071450 [+0, 1, -1, 0] 2
response to superoxide GO:0000303 [+0, 2, -1, 0] 3
UDP-N-acetylglucosamine biosynthetic process GO:0006048 [+0, 1, -2, 1] 4
transcription antitermination factor activity, RNA binding GO:0001072 [+0, 2, -2, 0] 4
sequestering of metal ion GO:0051238 [+0, 1, -1, 0] 2
negative regulation of DNA-templated transcription, termination GO:0060567 [+0, 1, -2, 0] 3
methylthiotransferase activity GO:0035596 [+0, 1, -1, 0] 2
purine nucleobase salvage GO:0043096 [+0, 1, -1, 0] 2
anaerobic glycerol catabolic process GO:0019588 [+0, 1, -1, 0] 2
fructose catabolic process GO:0006001 [+0, 1, -1, 0] 2
cellular response to superoxide GO:0071451 [+0, 1, -1, 0] 2
cellular oxidant detoxification GO:0098869 [+0, 1, -1, 0] 2
maintenance of location in cell GO:0051651 [+0, 1, -1, 0] 2
sequestering of iron ion GO:0097577 [+0, 1, -1, 0] 2
removal of superoxide radicals GO:0019430 [+0, 1, -1, 0] 2
intracellular sequestering of iron ion GO:0006880 [+0, 1, -1, 0] 2

Figure S1

proton-transporting two-sector ATPase complex GO:0016469 [+0, 6, -0, 2] 8
proton-transporting ATP synthase complex GO:0045259 [+0, 6, -0, 2] 8
isoleucine metabolic process GO:0006549 [+0, 5, -2, 0] 7
branched-chain amino acid biosynthetic process GO:0009082 [+0, 10, -3, 2] 16
isoleucine biosynthetic process GO:0009097 [+0, 5, -2, 0] 7
valine biosynthetic process GO:0009099 [+0, 6, -2, 0] 9
oxidoreduction-driven active transmembrane transporter activity GO:0015453 [+0, 2, -1, 1] 4
keto-3-deoxy-D-manno-octulosonic acid metabolic process GO:0046400 [+0, 3, -0, 1] 4
keto-3-deoxy-D-manno-octulosonic acid biosynthetic process GO:0019294 [+0, 3, -0, 1] 4
oxidoreductase activity, acting on a sulfur group of donors, NAD(P) as acceptor GO:0016668 [+1, 3, -0, 0] 5
energy coupled proton transmembrane transport, against electrochemical gradient GO:0015988 [+1, 4, -1, 1] 8
electron transport coupled proton transport GO:0015990 [+1, 4, -1, 1] 8
ATPase activity, coupled to transmembrane movement of ions, rotational mechanism GO:0044769 [+0, 6, -0, 2] 8
proton motive force dependent protein transmembrane transporter activity GO:0009977 [+0, 3, -0, 1] 4
imidazole-containing compound metabolic process GO:0052803 [+0, 5, -2, 1] 8
histidine metabolic process GO:0006547 [+0, 5, -2, 1] 8
histidine biosynthetic process GO:0000105 [+0, 5, -2, 1] 8
pyrimidine nucleobase biosynthetic process GO:0019856 [+1, 5, -0, 1] 8
'de novo' pyrimidine nucleobase biosynthetic process GO:0006207 [+1, 3, -0, 1] 5
organelle GO:0043226 [+1, 54, -2, 11] 75
non-membrane-bounded organelle GO:0043228 [+1, 54, -2, 11] 75
intracellular organelle GO:0043229 [+1, 53, -2, 11] 71
ribonucleoprotein complex GO:1990904 [+1, 47, -2, 7] 58
intracellular non-membrane-bounded organelle GO:0043232 [+1, 53, -2, 11] 71
intracellular ribonucleoprotein complex GO:0030529 [+1, 47, -2, 7] 58
ligase activity, forming carbon-oxygen bonds GO:0016875 [+2, 13, -0, 4] 19
ligase activity, forming aminoacyl-tRNA and related compounds GO:0016876 [+2, 13, -0, 4] 19
aminoacyl-tRNA ligase activity GO:0004812 [+2, 13, -0, 4] 19
tricarboxylic acid metabolic process GO:0072350 [+0, 4, -1, 1] 6
citrate metabolic process GO:0006101 [+0, 4, -1, 1] 6
tricarboxylic acid cycle GO:0006099 [+0, 4, -1, 1] 6
queuosine metabolic process GO:0046116 [+2, 3, -0, 0] 6
queuosine biosynthetic process GO:0008616 [+2, 3, -0, 0] 6
fatty acid binding GO:0005504 [+1, 3, -0, 0] 4
isopentenyl diphosphate metabolic process GO:0046490 [+0, 3, -0, 1] 4
isopentenyl diphosphate biosynthetic process GO:0009240 [+0, 3, -0, 1] 4
isopentenyl diphosphate biosynthetic process, methylerythritol 4-phosphate pathway GO:0019288 [+0, 3, -0, 1] 4
amino sugar biosynthetic process GO:0046349 [+1, 3, -0, 1] 5
UDP-N-acetylglucosamine metabolic process GO:0006047 [+1, 3, -0, 0] 4
UDP-N-acetylglucosamine biosynthetic process GO:0006048 [+1, 3, -0, 0] 4
aromatic amino acid family metabolic process GO:0009072 [+1, 5, -4, 3] 13
aromatic amino acid family biosynthetic process GO:0009073 [+0, 5, -4, 3] 12
erythrose 4-phosphate/phosphoenolpyruvate family amino acid metabolic process GO:1902221 [+0, 3, -0, 1] 4
erythrose 4-phosphate/phosphoenolpyruvate family amino acid biosynthetic process GO:1902223 [+0, 3, -0, 1] 4
L-phenylalanine metabolic process GO:0006558 [+0, 3, -0, 1] 4
aromatic amino acid family biosynthetic process, prephenate pathway GO:0009095 [+0, 3, -0, 1] 4
L-phenylalanine biosynthetic process GO:0009094 [+0, 3, -0, 1] 4
deoxyribose phosphate metabolic process GO:0019692 [+1, 2, -0, 1] 4
2'-deoxyribonucleotide metabolic process GO:0009394 [+1, 2, -0, 1] 4
deoxyribose phosphate biosynthetic process GO:0046385 [+1, 2, -0, 1] 4
2'-deoxyribonucleotide biosynthetic process GO:0009265 [+1, 2, -0, 1] 4
transcription antitermination GO:0031564 [+0, 7, -0, 1] 8
translation regulator activity GO:0045182 [+1, 4, -0, 0] 6
translation regulator activity, nucleic acid binding GO:0090079 [+1, 3, -0, 0] 4
translation repressor activity GO:0030371 [+1, 3, -0, 0] 4
translation repressor activity, nucleic acid binding GO:0000900 [+1, 2, -0, 0] 3
organelle GO:0043226 [+1, 54, -2, 11] 75
cytosolic part GO:0044445 [+3, 51, -3, 8] 69
ribosomal subunit GO:0044391 [+1, 45, -2, 7] 56
ribosome GO:0005840 [+1, 46, -2, 7] 57
intracellular organelle part GO:0044446 [+1, 45, -2, 11] 63
cytosolic ribosome GO:0022626 [+1, 45, -2, 7] 56
large ribosomal subunit GO:0015934 [+0, 25, -2, 5] 32
small ribosomal subunit GO:0015935 [+1, 20, -0, 2] 24
cytosolic large ribosomal subunit GO:0022625 [+0, 25, -2, 5] 32
cytosolic small ribosomal subunit GO:0022627 [+1, 20, -0, 2] 24
serine family amino acid biosynthetic process GO:0009070 [+1, 12, -0, 3] 17
homoserine metabolic process GO:0009092 [+1, 3, -0, 0] 4
homoserine biosynthetic process GO:0009090 [+1, 3, -0, 0] 4
mRNA binding GO:0003729 [+2, 10, -0, 1] 13
mRNA 5'-UTR binding GO:0048027 [+1, 4, -0, 0] 5
carbon-sulfur lyase activity GO:0016846 [+1, 7, -0, 0] 10
L-cysteine desulfhydrase activity GO:0080146 [+1, 3, -0, 0] 5
amino acid activation GO:0043038 [+2, 16, -0, 4] 22
protein stabilization GO:0050821 [+1, 3, -0, 1] 5
vitamin B6 metabolic process GO:0042816 [+0, 7, -0, 2] 9
ferric iron binding GO:0008199 [+1, 3, -0, 0] 4
nuclear chromosome segregation GO:0098813 [+0, 3, -0, 1] 4
tRNA aminoacylation GO:0043039 [+2, 15, -0, 4] 21
translation GO:0006412 [+4, 31, -0, 5] 45
rRNA binding GO:0019843 [+1, 21, -0, 4] 26
vitamin B6 biosynthetic process GO:0042819 [+0, 7, -0, 2] 9
pyridoxine metabolic process GO:0008614 [+0, 6, -0, 1] 7
amino acid kinase activity GO:0019202 [+1, 4, -0, 0] 6
intramolecular oxidoreductase activity, transposing S-S bonds GO:0016864 [+0, 2, -1, 1] 4
ribosomal small subunit biogenesis GO:0042274 [+0, 8, -0, 2] 10
sister chromatid segregation GO:0000819 [+0, 3, -0, 1] 4
heme-copper terminal oxidase activity GO:0015002 [+0, 2, -1, 1] 4
cis-trans isomerase activity GO:0016859 [+0, 6, -1, 1] 8
tRNA aminoacylation for protein translation GO:0006418 [+2, 15, -0, 4] 21
large ribosomal subunit rRNA binding GO:0070180 [+0, 5, -0, 1] 6
TAT protein transport complex GO:0033281 [+0, 2, -1, 1] 4
pyridoxine biosynthetic process GO:0008615 [+0, 6, -0, 1] 7
cyclohydrolase activity GO:0019238 [+0, 3, -0, 1] 4
aspartate kinase activity GO:0004072 [+1, 2, -0, 0] 4
protein disulfide isomerase activity GO:0003756 [+0, 2, -1, 1] 4
ribosomal small subunit assembly GO:0000028 [+0, 5, -0, 1] 6
sister chromatid cohesion GO:0007062 [+0, 3, -0, 1] 4
cytochrome bo3 ubiquinol oxidase activity GO:0009486 [+0, 2, -1, 1] 4
peptidyl-prolyl cis-trans isomerase activity GO:0003755 [+0, 6, -1, 1] 8
glycosyl compound biosynthetic process GO:1901659 [+2, 7, -0, 2] 12
RNA binding transcription factor activity GO:0001070 [+0, 3, -1, 0] 4
negative regulation of protein complex disassembly GO:0043242 [+0, 2, -1, 0] 3
oxidoreductase activity, acting on a sulfur group of donors, disulfide as acceptor GO:0016671 [+0, 7, -0, 1] 9
oxidoreductase activity, oxidizing metal ions GO:0016722 [+1, 3, -0, 0] 4
response to hydroperoxide GO:0033194 [+1, 2, -0, 1] 4
glucose metabolic process GO:0006006 [+3, 6, -0, 1] 12
nucleotide kinase activity GO:0019201 [+0, 5, -0, 1] 6
3'-5'-exoribonuclease activity GO:0000175 [+1, 3, -0, 0] 5
aminoacyl-tRNA editing activity GO:0002161 [+2, 4, -0, 1] 7
aldehyde biosynthetic process GO:0046184 [+0, 6, -0, 2] 8
acid-ammonia (or amide) ligase activity GO:0016880 [+1, 3, -1, 0] 6
nucleoside biosynthetic process GO:0009163 [+2, 7, -0, 2] 12
transcription antitermination factor activity, RNA binding GO:0001072 [+0, 3, -1, 0] 4
negative regulation of DNA-templated transcription, termination GO:0060567 [+0, 2, -1, 0] 3
hydroperoxide reductase activity GO:0032843 [+0, 3, -0, 1] 4
oxidoreductase activity, oxidizing metal ions, oxygen as acceptor GO:0016724 [+1, 2, -0, 0] 3
protein folding GO:0006457 [+1, 20, -0, 2] 28
structural constituent of ribosome GO:0003735 [+0, 3, -0, 1] 4
proline metabolic process GO:0006560 [+1, 2, -0, 1] 4
cytochrome o ubiquinol oxidase complex GO:0009319 [+0, 2, -1, 1] 4
protein transport by the Tat complex GO:0043953 [+0, 2, -1, 1] 4
RNA 3'-end processing GO:0031123 [+2, 2, -1, 0] 5
ammonia ligase activity GO:0016211 [+1, 1, -1, 0] 3
nucleoside triphosphate biosynthetic process GO:0009142 [+0, 3, -0, 1] 4
translation factor activity, RNA binding GO:0008135 [+1, 5, -0, 1] 7
peptide catabolic process GO:0043171 [+1, 5, -0, 0] 7
cytidylyltransferase activity GO:0070567 [+1, 3, -0, 0] 5
chaperone-mediated protein folding GO:0061077 [+1, 14, -0, 2] 20
protein disulfide oxidoreductase activity GO:0015035 [+0, 7, -1, 1] 10
carbon-nitrogen ligase activity, with glutamine as amido-N-donor GO:0016884 [+1, 4, -0, 0] 5
glutamine metabolic process GO:0006541 [+1, 3, -1, 0] 6
mRNA 3'-end processing GO:0031124 [+1, 1, -0, 0] 2
ncRNA 3'-end processing GO:0043628 [+1, 1, -1, 0] 3
aspartate-ammonia ligase activity GO:0004071 [+1, 1, -0, 0] 2
cation:amino acid symporter activity GO:0005416 [+0, 3, -0, 1] 4
ubiquinone binding GO:0048039 [+0, 4, -0, 1] 5
protein unfolding GO:0043335 [+1, 2, -0, 1] 4
lysine biosynthetic process via diaminopimelate GO:0009089 [+1, 5, -0, 1] 8
rRNA (cytosine) methyltransferase activity GO:0016434 [+0, 5, -0, 1] 6
uridylyltransferase activity GO:0070569 [+1, 3, -0, 0] 5
DNA topological change GO:0006265 [+1, 2, -0, 1] 4
3-hydroxyacyl-CoA dehydrogenase activity GO:0003857 [+1, 1, -1, 0] 4
glycerol metabolic process GO:0006071 [+1, 1, -1, 1] 4
mRNA polyadenylation GO:0006378 [+1, 1, -0, 0] 2
tRNA 3'-end processing GO:0042780 [+1, 1, -1, 0] 3
thiosulfate sulfurtransferase activity GO:0004792 [+1, 1, -1, 1] 4
deoxyribonucleotide catabolic process GO:0009264 [+1, 1, -0, 0] 2
polyol transport GO:0015791 [+3, 2, -0, 1] 6
D-alanine-D-alanine ligase activity GO:0008716 [+1, 1, -0, 0] 2
positive regulation of GTPase activity GO:0043547 [+1, 1, -0, 0] 2
phosphorylase activity GO:0004645 [+1, 1, -0, 0] 2
homoserine dehydrogenase activity GO:0004412 [+1, 1, -0, 0] 2
mRNA processing GO:0006397 [+1, 2, -0, 0] 3
asparagine metabolic process GO:0006528 [+1, 2, -0, 0] 3
energy reserve metabolic process GO:0006112 [+4, 1, -0, 1] 6
fructose-bisphosphate aldolase activity GO:0004332 [+1, 1, -0, 0] 2
cell redox homeostasis GO:0045454 [+2, 2, -0, 0] 5
maintenance of location GO:0051235 [+1, 1, -0, 0] 2
fatty acid synthase activity GO:0004312 [+1, 3, -0, 1] 5
organelle disassembly GO:1903008 [+1, 1, -0, 0] 2
ribonucleoprotein complex disassembly GO:0032988 [+1, 1, -0, 0] 2
lactate oxidation GO:0019516 [+1, 1, -0, 0] 2
RNA polyadenylation GO:0043631 [+1, 1, -0, 0] 2
asparagine biosynthetic process GO:0006529 [+1, 1, -0, 0] 2
glycogen metabolic process GO:0005977 [+4, 1, -0, 1] 6
peptidyl-serine autophosphorylation GO:0036289 [+1, 0, -1, 0] 2
sequestering of metal ion GO:0051238 [+1, 1, -0, 0] 2
3-oxoacyl-[acyl-carrier-protein] synthase activity GO:0004315 [+1, 1, -0, 0] 2
ribosome disassembly GO:0032790 [+1, 1, -0, 0] 2
malic enzyme activity GO:0004470 [+1, 1, -0, 0] 2
cellular response to cold GO:0070417 [+2, 1, -0, 0] 4
mRNA polyadenylation GO:0006378 [+1, 1, -0, 0] 2
lipopolysaccharide binding GO:0001530 [+1, 1, -0, 0] 2
rRNA (guanine-N7-)-methyltransferase activity GO:0070043 [+1, 0, -1, 0] 2
phosphotransferase activity, paired acceptors GO:0016781 [+1, 1, -0, 0] 2
maintenance of location in cell GO:0051651 [+1, 1, -0, 0] 2
sequestering of iron ion GO:0097577 [+1, 1, -0, 0] 2
intracellular sequestering of iron ion GO:0006880 [+1, 1, -0, 0] 2
polyamine biosynthetic process GO:0006596 [+0, 2, -2, 1] 5
spermidine metabolic process GO:0008216 [+0, 1, -2, 0] 3
amino acid import GO:0043090 [+0, 2, -3, 0] 6
tagatose-bisphosphate aldolase activity GO:0009025 [+0, 1, -1, 0] 2
DNA helicase complex GO:0033202 [+0, 2, -1, 0] 4
ADP-sugar diphosphatase activity GO:0019144 [+0, 1, -1, 0] 2
spermidine biosynthetic process GO:0008295 [+0, 1, -2, 0] 3
amino acid transmembrane import GO:0044745 [+0, 2, -3, 0] 6
arginine import GO:0090467 [+0, 1, -1, 0] 2
L-amino acid import GO:0043092 [+0, 1, -1, 0] 2
Holliday junction helicase complex GO:0009379 [+0, 1, -1, 0] 2
polysaccharide localization GO:0033037 [+0, 1, -3, 0] 5
heme transporter activity GO:0015232 [+0, 1, -1, 0] 2
leucine import GO:0060356 [+0, 1, -2, 0] 4
amino acid import across plasma membrane GO:0089718 [+0, 2, -3, 0] 6
L-arginine transmembrane transport GO:1903400 [+0, 1, -1, 0] 2
L-arginine import GO:0043091 [+0, 1, -1, 0] 2
3-deoxy-7-phosphoheptulonate synthase activity GO:0003849 [+0, 1, -2, 0] 3
polysaccharide transport GO:0015774 [+0, 1, -3, 0] 5
L-isoleucine transmembrane transporter activity GO:0015188 [+1, 1, -2, 0] 5
leucine import across plasma membrane GO:0098713 [+0, 1, -2, 0] 4
L-arginine import across plasma membrane GO:0097638 [+0, 1, -1, 0] 2
tryptophan synthase activity GO:0004834 [+0, 1, -1, 0] 2
acetolactate synthase activity GO:0003984 [+0, 2, -2, 1] 5
maltodextrin transport GO:0042956 [+0, 1, -3, 0] 5

Figure S2

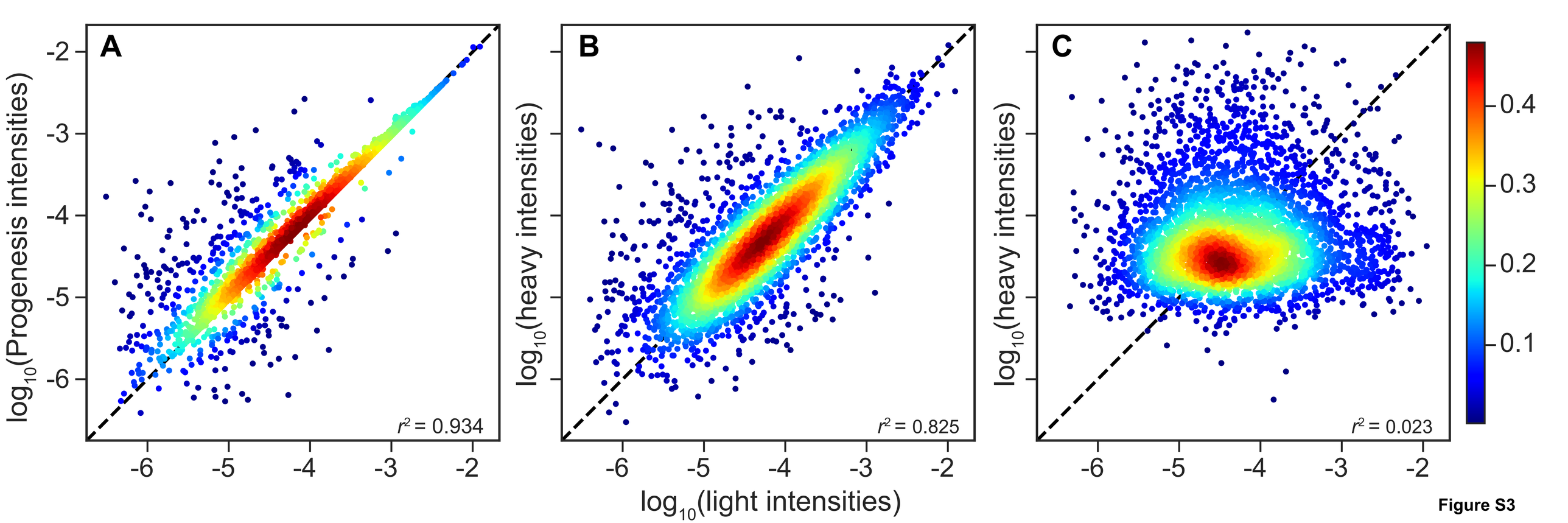
A
B
C
log10(Progenesis intensities)
log10(heavy intensities)
log10(light intensities)
r2 = 0.934
r2 = 0.825
r2 = 0.023
-2
-3
-4
-5
-6
0.4
0.3
0.2
0.1

Figure S3

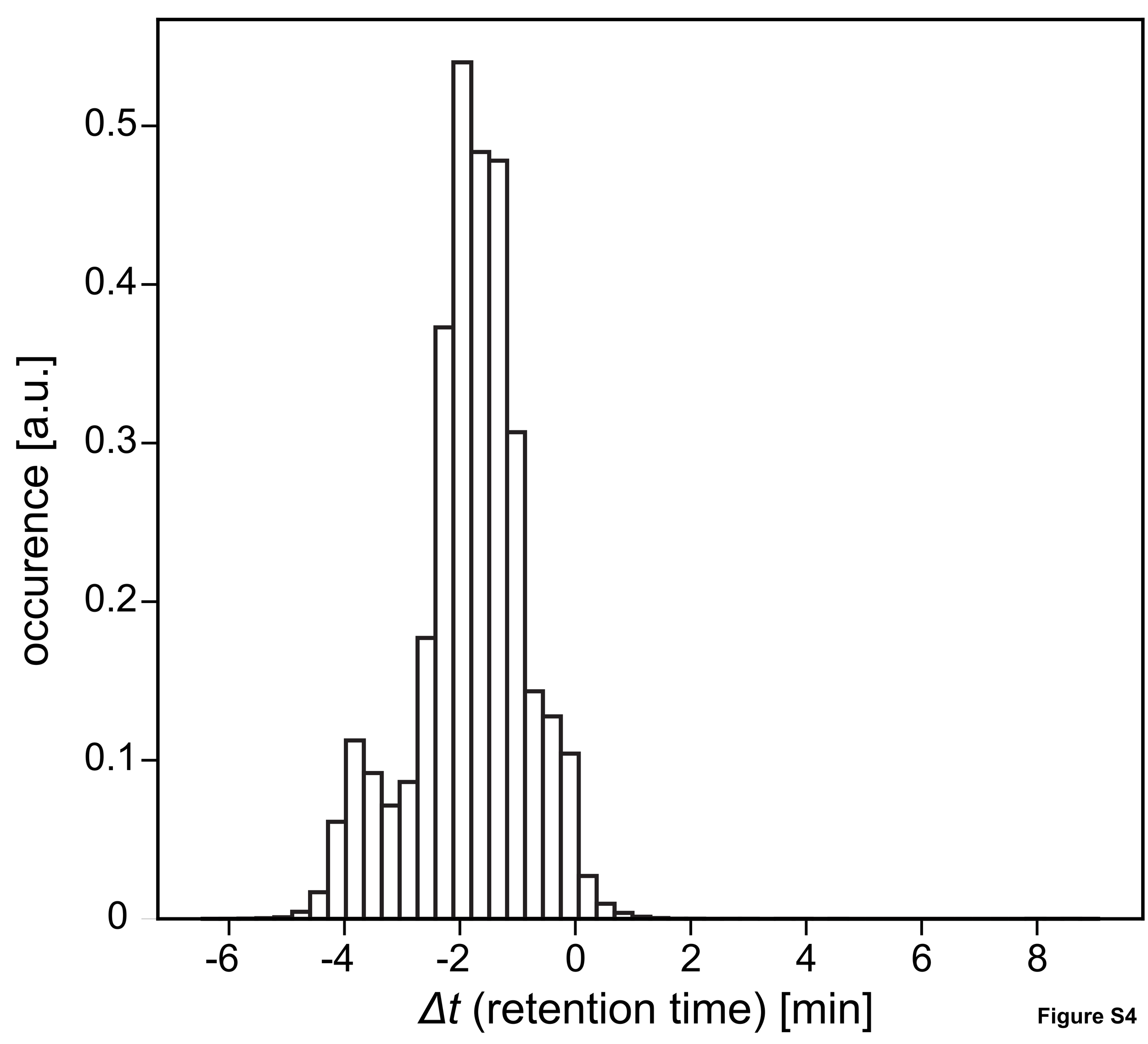

Figure S4